BOEING

D180-18475-1

RESEARCH STUDY ON HIGH ENERGY RADIATION EFFECT AND ENVIRONMENT – SOLAR CELL DEGRADATION METHODS

FINAL REPORT
CONTRACT NAS8-30378

Prepared for

George C. Marshall Space Flight Center
Marshall Space Flight Center, Alabama 35812

By W. E. Horne and M. C. Wilkinson

October 24, 1974
Nuclear & Space Physics Department
Boeing Aerospace Company
P. O. Box 3999
Seattle, Washington 98124

FOREWORD

This report is submitted to the National Aeronautics and Space Administration, George C. Marshall Space Flight Center, Huntsville, Alabama, in accordance with the requirements set forth in NASA contract NAS 8-30378. The work herein reported was performed by W. E. Horne and M. C. Wilkinson of the Boeing Aerospace Company, Nuclear and Space Physics Department, under the direction of K. D. Friddell.

ABSTRACT

A survey of proposed models for evaluating solar cell degradation has been made. It was found that the most widely utilized evaluation technique at present is based on empirically measured external damage coefficients. However, in recent years, the trend has been toward development of more detailed computerized analytical methods which utilize empirical data to deal with damage at the microscopic level inside the solar cell structure.

The most detailed and comprehensively verified analytical model has been used to evaluate the effects of simplifying assumptions on the accuracy of predictions made by the currently used external damage coefficient method. It was found that the most serious discrepancies were present in heavily damaged cells, particularly proton damaged cells, in which a gradient in damage across the cell existed. In general, it was found that the current damage coefficient method tends to underestimate damage at high fluences. An exception to this rule was thick cover-slipped cells experiencing heavy degradation due to omnidirectional electrons. In such cases the damage coefficient method overestimates the damage. Comparisons of degradation predictions made by the two methods and measured flight data confirmed the above findings.

CONTENTS

LIST OF FIGURES

1.0 INTRODUCTION

The radiation degradation produced in solar cells by the energetic charged particles of space is an important design constraint for many space missions. Since the original degradation estimates for Telstar[1] by Brown and Rosenweig, a series of reports sponsored by NASA[2], [3], [4] have reflected the development of increased environment definition and solar cell degradation understanding. These reports have treated the degradation of the solar cell primarily by bulk displacement damage through the use of an experimentally determined damage coefficient. This damage coefficient related the change in the cell diffusion length to the external particle fluence for each cell type. Cell performance parameters such as V_{oc}, I_{sc} and P_{max} were calculated from the new diffusion length. In this way solar cell degradation from various particle energies could be evaluated, and damage from differing particle types could be combined. However, the damage coefficient was found to be functionally dependent on numerous variables such as particle energy, particle fluence, operating temperature, light spectra, time, and etc. As more data were obtained it was found convenient to define separate damage coefficients for V_{oc}, I_{sc} and P_{max} for simplicity in describing observed cell degradation. Each of the coefficients in turn had functional dependencies on the variables mentioned above and were applicable only to the specific cell type measured. This rapidly expanding list of damage coefficient variables is very difficult to define experimentally and consequently many of the recognized variables have been treated with analytical approximations of varying degrees of credibility. The fundamental problem of low energy proton damage, which produces nonuniform damage in the cell, was always recognized as being beyond the capability of any simple damage coefficient method to treat accurately, and was thus a source of uncertainty. Also, such questions as the dependence of the damage coefficient on particle angle of incidence were also recognized but could receive no satisfying theoretical treatment.

The purpose of this work is to identify and quantify the uncertainties in the present techniques of solar cell radiation damage evaluation. The basic approach taken was first to search the literature on solar cell radiation evaluation, and then apply the most accurate technique available to specific solar cell radiation degradation problems.

Inherent in the external damage coefficient approach is the assumption that 1) radiation damage in the solar cell structure is uniform, and 2) that the effect of the damage on cell response is uniform across the cell. It is these assumptions that lead to many of the functional dependencies of the damage coefficients on such variables as fluence, light spectra, and particle angle of incidence. These assumptions also render the method inadequate in dealing with low energy proton damage which is very nonuniform within the cell. Further, the assumptions of uniformity of damage and response put limitations on the accuracy that can be expected in evaluating cell response to space radiation spectra which produce nonuniform damage profiles across the cells.

These problems have long been recognized and various models have been proposed to deal with the nonuniform damage production and response.

Two approaches[5], [6] to mathematical analysis of nonuniform damage were published in 1966. Both these approaches proposed the division of the solar cell base into sections or layers which could each be considered to be damaged to a different level. The continuity equations

1

were then solved to obtain the solar cell current and voltage. The results of these models were promising. A computerized model which could deal with the multilayered cell was reported in 1971.[7] Another attempt to deal with low energy proton damage was published in 1971.[8] This model used essentially the same mathematical approach with a defect damage coefficient defined to deal with the nonuniform dage within the cell on a microscopic basis rather than the macroscopic damage coefficients related to the external radiation field. Simultaneously, with the above efforts a computerized diode model called the PN code[9, 10] was developed under the sponsorship of the U. S. Air Force. This computer program became available in its present form about 1970. The code incorporates the layer approach in that the cell can be divided into twenty-six layers or segments. Having the varying parameters across the cell specified at the boundaries of the segments, the code interpolates to yield values of the parameters within the segments; thus, continuously varying parameters can be treated across the cell. The code also uses the defect damage coefficient concept to treat radiation damage on a microscopic level within the cell. The code was applied briefly to the problem of low energy proton damage in 1971.[11]

Thus, the trend in the literature has been the simultaneous development of a simplified, engineering data oriented model relating external radiation environments to cell response through empirical damage coefficients and a more detailed mathematical treatment of the cell relating damage internally in the cell on a microscopic level to solar cell response.

A recent work[12] has utilized the PN Code as a solar cell model and has drawn on a code from another discipline to deal with the omnidirectional radiation environment. A tested radiation transport code called SPARES (Space Radiation and Environment Code)[13] has been used to calculate the modified radiation spectrum inside the solar cell and yields displacement density profiles for use as input data in the PN Code.

As the defect density profiles can be obtained from the displacement density profiles, a calculation of displacement density in the cell resolves all the radiation environmental variables which complicate the solar cell radiation degradation problem. As tested transport codes for protons and electrons exist,[12] no significant errors are introduced in determining the penetrating proton or electron spectrum in the cell. The displacement damage cross section for protons and electrons has been evaluated by several workers[4], and is available for use. The displacement profiles produced by various environments and displacement cross sections can thus be compared.

The predictions of the P-N code for various proton and electron energies and cell types, based on the calculated displacement profiles in the cell, are compared to experimental results in Section 3.0 and Reference (12) to validate the basic diode simulation technique. Excellent agreement was obtained in nearly all cases examined, and low energy proton damage was also predicted accurately.

At the present time, this work appears to provide the most accurate, comprehensive method of solar cell evaluation found in the search of the literature and has had the most extensive validation with experimental data.

The current most widely used evaluation method is the external damage coefficient method. This method is attractive in that it can be made very simple and convenient for

2

designers to use. The remainder of this report shows the results of applying the detailed analytical method discussed above to evaluate the uncertainties introduced by simplifying assumptions that are inherent in the external damage coefficient method.

The analytical method was used to predict the radiation degradation in existing satellites and compare these predictions with flight data. A parametric study of degradation in common orbits of interest was then performed, and comparisons with the current damage coefficient method were made. This approach allowed the evaluation of simplifying assumptions made in the current damage coefficient radiation degradation method.

2.0 DETAILED RADIATION ENVIRONMENT EVALUATION

2.1 ENVIRONMENT DEFINITION

The trapped protons and electrons of the earth's radiation environment have been modeled by Vette and co-workers in a series of NASA reports[14] which remain the most accurate and comprehensive environment data available. The uncertainty in the models is a complex function of energy, position, and time for each particle type. As a broad guide a factor of 2 uncertainty in the proton maps and a factor of 3 to 5 in the electron environments has been used to characterize their accuracy. Solar proton activity cannot yet be predicted in a deterministic manner and the various projection of future proton activity based on correlation with sunspot activity or statistical consideration have large uncertainties for any time period of a few years or less. Solar panel degradation estimates from solar proton activity are based on a model proton environment suitable for the mission, and flight degradation data must be compared to degradation values calculated from the measured solar proton environment.

2.2 PROTON DISPLACEMENT DAMAGE EVALUATION

The determination of the displacement damage gradient in a cover glass-solar cell assembly proceeds in the following way. First the incident particle energy spectrum, fluence, and angle of incidence is found from the environmental definition. Then the penetrating particle energy spectrum and intensity is determined at several points in the solar cell. Finally the omnidirectional energy spectrum is combined with an energy dependent displacement production cross section to find the displacement density at each point of interest. This displacement density gradient, which can be expressed either in terms of a displacement production rate or for a total fluence as a total displacement damage gradient is then used as an input to the P-N diode model. The penetrating proton energy spectrum can be calculated for both normally incident or isotropically incident fluxes by the use of existing proton transport codes, such as those discussed in Reference (13). The Boeing HEVPEN code, developed and used in the SPARES code system, is used to evaluate the penetrating proton energy spectrum. The basic approximations used in this code are 1) neglect of nuclear interactions, and 2) neglect of scattering or straggling. These approximations introduce negligible error for the material depths of interest in solar cells. Typical penetrating proton spectra are shown in Figures 1 and 2 for normal incident proton spectra taken from AP-6 and AP-7 for 450 and 6000 nautical mile, 30° inclination circular orbits respectively.

2.3 TREATMENT OF ANGULAR DEPENDENCE

The penetrating proton spectra presented in the preceding figures show $\phi(E)$, the omnidirectional flux, calculated for a normally incident spectrum. To treat the space environment it is necessary to consider all angles of incidence. Define

Angular flux - $\phi(E, \Omega)$ particles/cm^2-MeV-steradian

Omnidirectional flux - $\phi(E)$ particles/cm^2-MeV

Number current – N(E)   particles/cm^2-MeV

Energy current – J(E)   MeV/cm^2-MeV

Now

$$\phi(E) = \int_\Omega \phi(E,\Omega)\, d\Omega = \int_0^{2\pi}\int_0^\pi \phi(E,\Omega)\, \sin\theta\, d\theta\, d\phi \qquad (2.1)$$

and

$$N(E) = \int_0^{2\pi}\int_0^\pi \phi(E,\Omega)\, \cos\theta\, \sin\theta\, d\theta\, d\phi \qquad (2.2)$$

The transport codes can be represented by a transmission function, T_r, which gives the energy and intensity of the particles after penetrating a thickness of material. A spherical shield of thickness x then gives a penetrating flux of

$$\phi(E) = \int_\Omega \phi(E,\Omega)\, T_r(E,\,x)\, d\Omega \qquad (2.3)$$

while for a slab, irradiated from one side

$$\phi(E) = \int_0^{2\pi}\int_0^{\pi/2} \phi(E,\Omega)\, T_r(E,\,\sec\theta\,x)\, \sin\theta\, d\theta\, d\phi \qquad (2.4)$$

For an isotropic angular distribution, the common approximation used for the complex angular dependence of the space environment,

$$\phi(E) = 4\pi\, \phi(E,\Omega)$$

and

$$N(E) = \frac{\phi(E)}{4} \text{ for a half space flux}$$

The actual penetrating spectrum from an omnidirectional fluence at various depths in a slab is given by Equation 2.4 as the weighted sum of each solid angle. For a displacement damage

5

calculation to evaluate the displacement damage at a point in the slab, it is necessary to know the omnidirectional fluence, $\phi(E)$, and the total displacement cross section, σ_D. The displacement density is then just

$$D_d = \int \phi(E) \ \sigma_D(E) \ dE \qquad (2.5)$$

The energy dependent function $\sigma_D(E)$ has been calculated by Baicker[15] for silicon and the values are given in Table 1. The methods discussed are then used to calculate displacement damage gradients in silicon for normal and isotropic fluxes taken from the two circular orbits.

2.4 ELECTRON DISPLACEMENT DAMAGE EVALUATION

The evaluation of electron displacement damage proceeds in the same way as for proton damage. The electron transport calculations are done with the Boeing electron Monte Carlo code EDEP[13], and the penetrating electron number current at various depths in silicon is calculated for either a normally incident or isotropically incident electron environment. The number current is converted into the omnidirectional flux by considering the angular distribution of the electron. The Monte Carlo method accounts for the effects of backscattering, energy and angle scatter resulting from the multiple scatterings that the electrons undergo in materials. The omnidirectional electron flux is combined with the energy dependent damage coefficient, $K(E)$ shown in Figure 3, to determine the damage gradients in silicon. The step of first calculating the total displacement density from a microscopic cross section is omitted since the electron damage coefficient is proportional to the displacement cross section in the energy region of interest.

The damage gradients in 10 ohm-cm silicon for 1-MeV electrons incident normally and isotropically in the half space are shown in Figure 4. Note that at the surface the damage is slightly greater for the isotropic flux because of increased backscatter. The normally incident damage curve shows an initial buildup, due to the scattering of the electrons from normal to a cosine squared angular distribution, and a gradual decline as the electrons are slowed to lower energies. In contrast the isotropically incident electrons have a constantly decreasing damage rate in the silicon. The synchronous altitude damage gradient is also shown in Figure 4.

Table I. Proton Total Displacement Production Cross Section in Silicon

E (MeV)	σ_D (Displacements/cm^3 per proton/cm^2)
0.1	80,000
0.3	26,000
0.6	13,000
1.0	8,000
3.0	2,600
6.0	1,600
10.0	1,300
30.0	850
60.0	500
100.0	260
200.0	120
1000.0	120

3.0 DETAILED PHYSICAL MODEL OF THE SOLAR CELL

3.1 GENERAL DISCUSSION OF MODEL

Examination of radiation damage models in the literature and results of exploratory testing have indicated the need for a detailed physical model which could account for variations in internal physical parameters rather than consider the device as a homogeneous structure beneath the junction. The model also needs to be able to handle a nonuniform carrier generation rate across the cell such as that due to the sun spectrum and to be able to account for radiation induced recombination centers whose energy levels within the band gap were different than those responsible for initial recombination before radiation.

Some of the observations that indicate the above requirements are: 1) nonuniform damage rates due to particle spectra in space, 2) nonuniform annealing in lithium doped solar cell structures, 3) fluence dependence of damage coefficients at fluences too low to cause significant carrier removal, 4) temperature dependence of damage coefficients, 5) nonuniform carrier generation rates resulting from the solar spectrum, and 6) the effects of drift fields within the cell due to nonuniform impurity profiles.

Calculations of the defect density profiles due to particle spectra in space indicate that relatively steep gradients in damage, or defect density, can be introduced in the solar cell structure; therefore damage coefficients based on external measurements in monoenergetic radiation fields place an undesirable limitation on ones ability to assess orbital effects--particularly in the case of protons which are stopped within the solar cell or for cells which have built-in electric fields.

As will be discussed later, nonuniform annealing across the base region of lithium doped cells can result in further complications of the damage profile and can change the dopant impurity profile in the device. Alterations of the impurity profile can result in changes of the built-in electric field due to lithium donor impurity gradients near the junction. Annealing of nonuniform damage densities resulting from the space environment can further complicate this situation. Thus a model which can deal with an inhomogeneous cell is a necessity.

Fluence dependence of external damage coefficients can result from severe degradation of the diffusion length in the solar cell base. This effect appears to be due to the difference in spectral response of the cell and is particularly evident in cells having built-in electric fields.

Damage coefficients have been observed to be temperature dependent for cells. Faith[16] presented an analysis of this temperature dependence in which he related it to the energy level of the radiation induced recombination center with respect to the location of the Fermi level within the band gap. He presented comparisons of temperature dependence calculations based on the energy levels of several known recombination centers and experimental data. Based on these results he concluded that the damage could not be singularly identified with any particular center but rather was probably due to a composite of two or more centers. This conclusion is in agreement with the findings of Carter[17] regarding damage introduction by electrons of different energies, namely that the "A" center appeared to be important in N/P cells for electron energies

7

below the one MeV and "K" centers more important at higher energies. Thus, it is necessary that a complete model be able to account for the energy level of the radiation induced recombination centers.

It is well recognized that the difference in response of solar cells to light of various wavelengths make the effects of radiation a function of the light spectra. Thus, it is essential that the model be able to consider the actual light spectrum of interest.

The presence of a built-in electric field due to a gradient in dopant impurity profile can radically alter the response of a solar cell. Thus, defects in different locations in such a device vary in their effect on the cell output.

All of the above considerations make a detailed physical model of the solar cell (which can deal with variations in parameters throughout the cell) very desirable, indeed, essential, in order to accurately assess the effects of the space environment throughout an orbital mission.

The PN Code developed by Gulf Radiation Technology for the Air Force Weapons Laboratory[10] appeared to have most of the above listed qualities. The mechanics of the code have been described in the literature[9, 10]; therefore, only a description of its capability pertaining to solar cells will be presented in this report.

The basic equations that are solved by the computer for the interior of the device are the one-dimensional continuity equations for the two charged carriers, n and p,

$$\frac{\partial n}{\partial t} = g - R + A - \frac{\partial J_n}{\partial x} + g_{n'}$$

(3.1)

and

$$\frac{\partial P}{\partial t} = g - R + A - \frac{\partial J_p}{\partial x} + g_{p'}$$

(3.2)

and Poisson's equation for the electric field E,

$$\frac{\partial E}{\partial x} = \frac{4\pi q}{K} [p - n + \Delta N].$$

(3.3)

In these equations, n is the density of the negatively charged carrier and p is the density of the positively charged carrier. Terms g and A are the generation rates of electron-hole pairs caused by external radiation and avalanche, respectively; R is the recombination rate of electrons and holes; and g_n and g_p are the rates at which electrons and holes are injected at certain places into the device, for example, by the base contact or tunneling. In Eq. 3.3, N is the net density of doping, positive for donors and negative for acceptors; q is the absolute charge of an electron (positive); and K is the dielectric constant. The terms J_n and J_p are the particle current densities:

$$J_n = -n\mu_n E - E_n \frac{\partial n}{\partial x} n v_n - D_n \frac{\partial n}{\partial x'}$$

(3.4)

and

$$J_p = p\mu_p E - D_p \frac{\partial p}{\partial x} = pv_p - D_p \frac{\partial n}{\partial x}, \qquad (3.5)$$

The E (or velocity v) terms are the drift currents with mobilities μ_n and μ_p and the $\partial/\partial x$ terms are the diffusion currents with diffusion coefficients D_n and D_p. The terms g, A, R, μ_n, μ_p, D_n, and D_p are functionally dependent on position, time, densities, and electric fields for semi-conductors. In most of the following, tunneling will be assumed negligible so the g_n and g_p terms are due only to the injection or removal of carriers by the base contact. Two sets of boundary conditions are available for the solution of Equations 3.1 through 3.5.

Type I boundary conditions are sometimes called "bulk" boundary conditions because they correspond to conditions far from any discontinuity in the doping. Specifically, the Type I boundary conditions are:

$$\frac{n}{x} = \frac{p}{x} = 0, \qquad (3.6)$$

and

$$q(n\mu_n + p\mu_p) E + \frac{\kappa}{4\pi} \frac{\partial E}{\partial t} = \frac{i}{a_o}, \qquad (3.7)$$

at both ends of the device. The function i is the external current at the appropriate end of the device, and a is the cross-sectional area of the one-dimensional device. Equation 3.7 is just Maxwell's equation for continuity of total current, including the displacement current $\partial E/\partial t$. Type I boundary conditions are applicable to problems where the details of the contacts do not significantly affect the results. Consequently, Eq. 3.7 does not include the effect of carrier tunneling between the metal and semiconductor.

Type II boundary conditions are necessary when the details of the contacts to the device are important. A typical situation where they would apply is the study of metal-semiconductor contacts. Specifically, the Type II boundary conditions are:

and

$$\left.\begin{array}{l} n = \text{constant with time,} \\ \\ \\ \\ p = \text{constant with time,} \end{array}\right\} \qquad (3.8)$$

$$q(n\mu_n E + p\mu_p E + D_n \frac{\partial n}{\partial x} - D_p \frac{\partial p}{\partial x}) + \frac{\kappa}{4\pi} \frac{dE}{dt} = \frac{(i - i_t)}{a_o}, \qquad (3.9)$$

at both ends of the device. The term i_t is the tunneling current between the metal and the semiconductor at the appropriate end of the device.

9

It will be noted that Eq. 3.7 is just a special case of Eq. 3.9 in which $\partial n/\partial x$, $\partial p/\partial x$, and i_t have been set equal to zero. In general, n and p at a given boundary are not equal and their values at the two boundaries may be different. Also, the code can consider Type I boundary conditions on one surface and Type II on the other, if desired.

The program is capable of solving the equations 1 through 5 for a multiple region diode structure. The solar cell structure can be divided into as many as twenty-six regions. The width of the regions can be varied throughout the cell structure. For example, in a location where parameters such as dopant impurity density or radiation defect density are varying rapidly, several very narrow regions can be defined to adequately describe the parameters where parameters are varying more slowly, the regions can be made very wide. Values of the parameters are input into the code for the region boundaries and the program interpolates for values within the region boundaries.

Examples of parameters which are put into the code as a function of position are: 1) electron and hole mobility, 2) carrier generation rates, 3) dopant impurity densities, 4) electron and hole lifetimes, 5) carrier densities in the conduction and valence bands when the Fermi level coincides with the energy level of the recombination centers, 6) intrinsic carrier densities in the conduction and valence bands at the temperature of interest, 7) radiation defect introduction rates, etc. Thus, the model accounts for inhomogeneities throughout the cell. The model also accounts for electric fields within the device due to dopant impurity gradients.

The subroutine which accounts for radiation damage within the solar cell uses the equation

$$
R = \frac{nP - n_{f_1} P_{f_1}}{\tau_{no_1}(P + P_{f_1}) + \tau_{po_1}(n + n_{f_1})} + \frac{nP - n_{f_2} P_{f_2}}{\tau_{no_2}(P + P_{f_2}) + \tau_{po_2}(n + n_{f_2})} \tag{3.10}
$$

where R is the recombination rate, n and P are the electron and hole densities respectively, τ_{no}, is the initial electron lifetime, τ_{no2} is change in lifetime due to radiation induced recombination centers, τ_{po1} and τ_{po2} are similar quantities for hole lifetimes, n_{f_1} and n_{f_2} are the electron densities in the conduction band when the Fermi level coincides with the recombination centers associated with each case, and P_{f_1} and P_{f_2} are similar quantities for holes. The first term having 1 subscripts represents the initial recombination term before radiation while the 2 subscripted term represents recombination due to radiation damage. Temperature dependence of the radiation damage is due primarily to the terms n_{f_2} and P_{f_2} which can be expressed by

$$
n_{f_2} = N_c e^{-(E_c - E_r)/kT} = k_e T^{(3/2)} e^{-(E_c - E_r)/kT} \tag{3.11}
$$

and

$$
P_{f_2} = N_v e^{-(E_c - E_r)/kT} = k_v T^{(3/2)} e^{-(E_r - E_v)/kT} \tag{3.12}
$$

10

where N_c and N_v are the number of allowed states in the conduction and valence bands respectively, E_c and E_v are the conduction and valence band energy levels, E_r is the recombination center energy level, k_c and k_v are constants of proportionality, K is Boltzmann's constant and T is the temperature in degrees Kelvin.

The terms τ_{no_1} and τ_{po_1} represent the limiting lifetimes in highly n-type and highly p-type silicon and can be expressed by

$$\tau_{no_1} = \frac{1}{N_1 \, \sigma_{n1} \, V_n} \text{ and } \tau_{po_1} \frac{1}{N_1 \, \sigma_{p1} \, V_p} \qquad (3.13)$$

where N_1 is the density of recombination centers present σ_{n1} and σ_{p1} are the capture cross sections for electrons and holes respectively and V_n and V_p are the thermal velocities of electrons and holes respectively. Before irradiation the recombination centers are due primarily to natural defects in the crystalline structure and to trace impurities. These centers are usually deep within the band gap and for purposes of this study have been assumed to be at the center of the band gap.

The terms τ_{no2} and τ_{po2} can be expressed by

$$\tau_{no_2} = \frac{1}{N_2 \, \sigma_{n2} \, V_n} \text{ and } \tau_{po_2} \frac{1}{N_2 \, \sigma_{p2} \, V_p} \qquad (3.14)$$

where N_2 is the density of recombination centers introduced by radiation and σ_{n2} and σ_{p2} are the capture cross sections of these defects.

Multiple defects may be represented by additional terms or they can be approximated by a composite energy level that represents the composite effect of the different centers. The latter approach has been used in the present study and found quite adequate.

The radiation damage is represented in the PN Code by two constants in the following manner

$$\tau_{on2} = \frac{1}{N_2 \, \sigma_2 \, V_n} = \frac{K_n}{K1\Phi} \qquad (3.15)$$

where K_n is a defect lifetime damage coefficient, $K1$ is the defect introduction rate, and Φ is the radiation fluence. Thus, the code requires the constants K_n and $K1$ as inputs. Φ is calculated by integrating the particle flux $d\Phi/dt$ (which is an input requirement) over the time interval of interest (another input).

3.2 ELECTRON DAMAGE INTRODUCTION

The radiation degradation is introduced into the diode model by a second recombination term as shown in Equation 3.2. This term differs from the initial recombination term in that n_f and P_f are determined by the energy level of the radiation-induced recombination center and the parameter τ_{on} and τ_{op} vary as the density of recombination centers is increased by the radiation flux.

11

For purposes of this example, consider an N/P type cell. The radiation damage degrades the minority carrier lifetime by introducing recombination centers at several energy levels within the band gap. The effect of these centers on the recombination rate is introduced into the solar cell model through the term τ_{on2} in Equation 3.2. τ_{on2} is dependent on the number of radiation centers by the relation

$$\tau_{on2} = \frac{1}{N_2 \, \sigma_2 \, V} \tag{3.16}$$

where N_2 is the number of radiation centers, σ_2 is the electron capture probability of the centers and V is the thermal velocity of carriers. In the diode model a constant K_p is defined which accounts for $\frac{1}{\sigma_2 V}$ in Equation 3.8. This constant is in effect a defect lifetime damage coefficient. The number of centers N_2 is accounted for by a constant K_1 which multiplies the radiation fluence and is the defect introduction rate. Thus the effect on lifetime requires two input parameters as shown by

$$\tau_{on} = \frac{K_p}{K_1 \Phi} \tag{3.17}$$

The introduction rate varies for the different types of centers and since all the centers probably result in some recombination the constant K_1 has been considered a composite introduction rate which approximates the effect of all the centers. The alternative to this approach would require recombination terms for each center and, hence, introduction rates and defect lifetime damage coefficients for each center. The situation is further complicated in that the energy dependence of introduction of the various centers may be different. For these reasons, considering the composite effect of the centers seemed more practical and appears to yield sufficiently adequate results. Having made this decision the values of K_1 and K_p become interdependent in that one must be known in order to calculate the other. K_1 becomes more important when annealing is considered later. For purposes of this example K_1 was taken to be the introduction rate of the $E_v + 0.3$ ev center whose energy dependence has been observed to be similar to that of electron damage in N/P type cells.[13] The introduction rate used was 0.25 cm^{-1} for 10 MeV electrons. The constant K_p is then calculated by means of the relationship

$$K_p = \frac{D K_L}{K_1 \Phi} \text{ where } \frac{1}{L^2} - \frac{1}{L_o^2} = K_L \Phi \tag{3.18}$$

at several fluences. The value calculated at $\Phi = 10^{14}$ e/cm^2 (10 MeV) was found to be $K_p = 1.65 \times 10^{-7}$ cm^{-1}.

The energy level assumed for the defect becomes important in that the temperature dependence of the recombination center is determined by the energy level. This is reflected through the terms n_{f_2} and P_{f_2} in Equation (2). The composite energy level is determined by comparisons of calculations of the term expressed in Equation (3) and the experimentally measured temperature dependence of damage from the monoenergetic electrons. Figure 5 shows a comparison

12

of the calculated and measured short circuit current degradation at different temperatures using a composite energy level of $E_v + 0.20$. Figure 6 shows a comparison of calculated IV curves with experimental data at several fluences of 10 MeV electrons.

3.3 PROTON DAMAGE INTRODUCTION

The proton damage model to be used in the evaluation is similar to the electron damage model. It is assumed that the defects consist primarily of point defects and that their density varies along the path length of the proton according to an 1/E type cross section below about 15 MeV.

Such an approach was suggested as early as 1970[8]; however, in that work the lack of a generalized diode model restricted it to uniform generation rates (long wavelength light spectra). Such an approach is inherent in the PN Code model as described in the electron damage section. The PN Code was applied briefly to the problem of proton damage in 1970. [11] The present work has gone into a more rigorous verification of the validity of the approach.

One of the main problems in such an approach is determining the defect lifetime damage coefficient and defect introduction rate. No conclusive works have been found in the literature regarding the introduction rate of recombination centers along the proton path length. As was stated in the case of electron damage, the defect lifetime damage coefficient and introduction rate are interdependent in the sense that once one is established then the other is determined by

$$k_p = \frac{K_L}{K_1 \Phi}$$

(3.19)

where K_L is the macroscopic lifetime damage coefficient determined externally for cases of uniform damage in the solar cell base and $K_1 \Phi$ is the product of the defect introduction rate and the total fluence.

For proton damage, neither K_1 of k_p have been determined uniquely from experiments. For purposes of this study the constant k_p is assumed equal to that for electron damage and the damage introduction rate calculated from 15 MeV proton damage. The energy of 15 MeV was chosen as being low enough to still follow 1/E type dependence on energy yet high enough to produce relatively uniform damage across the solar cell. Thus, in P type material (N/P type cell) the short circuit current ratio I_{sc}/I_{sco} was 0.88 at 1×10^{11} P/cm^2 (15 MeV) and L was measured to be approximately 70 μm. Thus,

$$\frac{1}{(7 \times 10^{-3})^2} - \frac{1}{(1.4 \times 10^{-2})^2} = K_L (1 \times 10^{11}) \text{ P/cm}^2 \quad \text{or}$$

(3.20)

$$K_L = 1.54 \times 10^{-7} \quad \text{the } K_1 = \frac{K_L}{K_p} = \frac{1.54 \times 10^{-7}}{1.65 \times 10^{-7}} = .935$$

(3.21)

13

The value of K_1 at 15 MeV is then compared to the curve for absolute defect density shown in Figure 7. If the distribution of recombination centers along the proton track is assumed to have the same profile as the absolute displacement density then the curve of Figure 7 can be normalized to the value of recombination centers at 15 MeV and used to yield the introduction rate for other energy particles.

4.0 COMPARISON OF RADIATION DAMAGE PREDICTION METHODS

To compare the results of the external damage coefficient radiation damage model, presented in the current form in the TRW handbook and the analytical method just presented, the predictions of the two methods for various specific orbits were worked out. First predictions for several satellite for which flight data is available were made. Then three typical missions, 450 N.M. and 6000 N.M. circular 30° inclination orbits, and a synchronous altitude electron environment were compared. Finally the differences in the prediction methods were examined and explained where possible.

4.1 FLIGHT DATA COMPARISON

In the TRW Handbook[4] flight degradation data on several satellites are presented and compared with the handbook method damage predictions. For purposes of comparison solar cell damage estimates have been prepared based on the orbit parameters and solar panel data presented in the handbook by the use of the analytical damage prediction technique. The displacement density gradient in the 40 mil cover slip and 18 mil cell of Explorer 38 are shown in Figure 8. Predictions of panel degradation are shown in Figure 9 for Explorer 38 and for several other satellites in Figure 10. Error bars on the flight data was not available. The trend is for more degradation to be observed than predicted by the external damage coefficients. Agreement is good between the flight data and the analytical method. This result supports the monoenergetic electron and proton experimental data and prediction method agreement shown in the previous section, and also indicates that the actual displacement gradients produced in space missions are being treated accurately in the analytical method.

4.2 SPECIFIC ORBIT ANALYSIS

Two near earth trajectories, 450 and 6000 N.M. circular, 30° inclination, were then examined to determine the differences between prediction methods and to examine the importance of the displacement damage gradients. The 450 N.M. orbit sees a hard proton energy spectrum and would produce a minimum damage gradient, while the 6000 N.M. orbit sees a soft proton energy spectrum with a large damage gradient across the cell. In addition to the nominal 1-MeV electron degradation data presented in the TRW Handbook, the P-N code was used to calculate 1-MeV electron degradation data. This data is compared in Figures 11 and 12 for I_{sc}/I_{sco} and V_{oc_o}/V_{oc}. This P-N code determined 1-MeV degradation data, which agrees with BREL test data, Reference 12, can be used to separate differences in degradation prediction resulting from variations in nominal cell characteristics.

4.2.1 450 N.M. Circular

Figures 13 and 14 show the predicted degradation in this orbit for V_{oc} and I_{sc} as a function of time. V_{oc} is predicted to degrade more severely by the analytical method than by the external damage coefficient technique. The 1-MeV electron degradation curve calculated by the P-N code degrades at the same rate as does the analytical method prediction, indicating an increase in external damage coefficients would result in better agreement. This increase is a factor of 1.7.

I_{sc} is predicted to degrade more severely, and at a greater rate by the analytical method than by the external damage coefficient method. This shows the importance of the damage gradient across the cell, which result in greater I_{sc} degradation in the space environment. It is logical that displacement damage gradients which differ as much as the 1-MeV electron and 450 N.M. proton environment would result in differing degradation rates. Differences in I_{sc} degradation imply that the entire I-V curve would have a different shape for 1-MeV electron and space proton radiation degradation.

4.2.2 6000 N.M. Orbit

This orbit has a softer proton spectrum, and hence a steeper damage gradient than the 450 N.M. orbit. The difference in V_{oc} and I_{sc} degradation shown in Figures 15 and 16 are therefore similar, but accentuated from the previous orbit. V_{oc} degradation occurs in 1/2 the time predicted by the external damage coefficient method compared to the analytical method. The difference in I_{sc} degradation rates is also greater.

4.2.3 Synchronous Altitude Electrons

A similar comparison program was made for the synchronous altitude electron environment. Less damage was found for the analytical method compared to the external damage coefficient predictions, with slightly different degradation rates. This is understandable when one considers the much shallower damage gradient produced by the space electrons. It appears that the magnitude of the degradation is influenced by the treatment of electron angular dependence, discussed in the next section.

5.0 DETAILED PREDICTION TECHNIQUE COMPARISON

The previous section has compared the radiation damage prediction methods on an integral basis for specific missions and solar panel configuration. We now examine in detail some differences in the treatment of environmental and solar cell parameters.

5.1 ENVIRONMENTAL EVALUATION

The treatment of the angular dependence of the incident protons or electrons differs between models. The analytical method calculates the displacement density in a straightforward way, with no approximations needed that introduce any significant errors. The external damage coefficient method treats high energy protons and electrons as having damage coefficients that are independent of angle of incidence, while low energy protons are treated by a complex approximation that attempts to conserve the total number of displacements produced in the cell by a stopping proton of any angle of incidence. By examining Figures 17 and 18, the displacement density gradients calculated by the HEVPEN code for 450 and 3000 N.M. proton spectra can be used to evaluate these assumptions for a typical space proton environment. First, the ratio between the normal incidence and isotropic incidence displacement densities at 0 thickness is just a factor of two, the ratio of the omnidirectional fluxes. This corresponds to the assumption of no dependence on angle of incidence made for high energy protons. For increasing material thicknesses, this ratio gradually increases until, at a depth of .14 g/cm^2, ~12 mils, it reaches 3.5. Since the energy current into the cell differs between normal and isotropic incidence by a factor of four, and since the fraction of incident proton energy used in producing displacement damage is independent of angle of incidence, the total number of displacements produced in an infinite thickness of silicon by normal and isotropic incident fluxes differ by a factor of four. The normal to isotropic displacement density ratio must then always drop below four at some depth to compensate for the lower surface ratio. For typical solar cell cover slip thickness, 6 to 12 mils, the normal to isotropic displacement density ratio is greater than two indicating that the fraction of displacement damage resulting from high energy protons, where the angle independent damage approximation is reasonable, is small for the proton environments of space.

Electron damage coefficients have been assumed independent of incident angle, based on the experimental results of Barrett[18] and the penetrating nature of electrons in the MeV energy range. Figure 4, which compares the displacement gradients in silicon for normal and isotropic in the half space 1-MeV electron fluxes, shows that the near surface displacement ratios are similar but the isotropic displacement curve drops away from the normal incident value at greater thicknesses. The analytical method will then predict proportionally less damage with increasing cover glass thickness. The experimental data of Barrett, taken on bare cells at incident angles of up to 60°, did not explore the angles of incidence and depths of material where the angular dependence of the damage coefficient could be observed. That such a dependence must exist is obvious from the energy conservation argument used for protons. Since the isotropic in the half space flux only results in one half the energy current as a normal incident flux, the displacement density gradients must diverge in the material. Backscattering increases the energy loss of the isotropic flux compared to a normal flux.

The general shape of the proton total displacement cross section curve can also be compared with the energy dependent damage coefficient curves. In Figure 19 we show the damage coefficient data obtained by Meulenberg and Treble[19] and the In E/E displacement cross section. The two basic differences are the plateau at 10 to 30 MeV energy in the damage coefficient curve, and the low energy roll off. The low energy roll off in the damage coefficient curve is a result of the non-uniform damage gradient produced in solar cells by low energy protons. As such, it has an inherent fluence dependence, and cannot be compared directly to the displacement cross section. The importance of an accurate treatment of this low energy proton energy range is shown in Figures 17 and 18 where the displacement density produced by protons of less than 1-MeV is given as the difference between σ_{D1} and σ_{D2} for the two orbital altitudes. A significant fraction of the displacements are produced by these low energy protons.

The plateau in the damage coefficient curve, shown in Figure 19, is only partly described by the optical model cross section calculations of Baicker. Whether including the inelastic reaction such as (p, d), (p, t), and (p, He) would explain this hump, or whether damage cluster effects are present as suggested by Treble and Meulenberg is not yet known. For the evaluation of space proton damage the great importance of low energy protons tends to reduce the importance of the 10-30 MeV energy region.

6.0 CONCLUSIONS

The comparison calculations made in this work lead to the following general conclusions about the accuracy of the current solar cell damage evaluation method using external damage coefficients.

1) Low Energy Proton Damage Is Underestimated at High Fluences

The comparison results for both 450 and 6000 N. M. orbits show that the cell degradation in both V_{oc} and I_{sc} is underestimated by current methods. This underestimate becomes larger with increasing fluences. As it has been shown that low energy protons (< 10 MeV) are most numerous in the penetrating space environment, it is concluded that low energy proton damage is underestimated. These results were obtained with 6 mil cover slips. For thicker cover slips, we expect the penetrating proton energy spectrum to harden and reduce the importance of the low energy proton damage. For thinner cover slips, the low energy proton damage would be increased.

2) Damage gradient produced by space proton spectra places a serious limitation on the 1 MeV equivalent damage coefficient method at high fluences.

The damage gradients produced in solar cells by space proton spectra result in underestimates of cell degradation at high fluences when the assumption of uniform damage is made as is the case for the external damage coefficient method. As shown for the 450 and 6000 N. M. orbits, the degradation in I_{sc} proceeds at a faster rate when calculated by the analytical method than when calculated by external damage coefficients. This systematic variation, which is proportional to the displacement damage gradient in the cell cannot be corrected by adjusting the external damage gradients but is an essential result of the displacement damage gradient in the cell. These results were obtained for 6 mil cover slips. Increasing the cover slip thickness will reduce the damage gradients in the cell.

3) Electron Degradation Is Overestimated by the External Damage Coefficient Method

The assumption that the electron damage coefficient is independent of angle of incidence leads to an overestimate of the degradation. The magnitude of this effect is not large since the difference between the normal and isotropic incident electron damage gradients at 6 mils (the cover slip thickness) is not large. However, the difference would increase with increasing cover slip thickness.

4) Finally, the general conclusion may be drawn that for missions where heavy damage is expected (particularly proton damage), the current external damage coefficient method is inadequate. A more detailed analytical treatment which can account for damage gradients across the cell is required.

7.0 RECOMMENDATIONS

To increase the accuracy of solar cell degradation estimates for both conventional N/P and recently developed cell types such as the COMSAT Violet Cells or the K-6 cell, and to examine the improvements possible in solar cell radiation hardness, the following steps are recommended.

1. Develop accurate degradation data on N/P cells for various cover slip thicknesses and orbits by using the analytical degradation prediction method.

2. Evaluate recently developed cell types, such as the COMSAT Violet Cell and the Hughes K-6 cell, in the space environment by the analytical degradation prediction method.

3. The analytical degradation prediction method should be used to examine the effectiveness of various solar cell radiation hardening techniques in the space environment.

8.0 REFERENCES

1. W. Brown, J. Gabbe and W. Rosenzweig, Results of the Telstar Radiation Experiment, the Bell System Technical Journal, July 1963.

2. W. C. Cooley and R. J. Janda, Handbook of Space-Radiation Effects on Solar-Cell Power Systems, Exotech, Inc., NASA SP-3003, 1963.

3. W. C. Cooley and M. J. Barrett, Handbook of Space Radiation Effects on Solar Cells, Exotech, Inc., TR-025, 1968.

4. J. R. Carter, Jr. and H. Tada, Handbook of Space Radiation Effects, Final Report, Contract JPL 953362, Prepared by TRW, June 1973.

5. H. Y. Tada, "A Theoretical Model for Low-Energy Proton Irradiated Silicon Solar Cells", Proceedings of the Fifth Photovoltaic Specialists Conference, Vol. II, January, 1966.

6. D. Crowther, et al., "An Analysis of Non-Uniform Proton Irradiation Damage in Silicon Solar Cells", IEEE Transactions on Nuclear Science, October, 1966.

7. M. J. Barrett, et al., "Solar Cell Performance Mathematical Model", Final Report, JPL Contract 952548 prepared by Exotech, Inc., June, 1970.

8. I. Nashiyama, et al., "Protons and Deuteron Irradiation Damage in Silicon Solar Cells", Japanese Journal of Applied Physics, Vol. 10, No. 11, November, 1971.

9. R. E. Leadon and M. L. Vaughn, "Short-Pulsed Radiation Effects on Dynamic Electronic Components", Final Report, Contract DASA 01-68-C-0123, Prepared for Defense Atomic Support Agency by Gulf General Atomic Incorporated, June, 1969.

10. R. E. Leadon, et al., "Radiation Effects on Dynamic Electronic Components, Final Report, Contract DASA 01-69-C-0113, Prepared for Defense Atomic Support Agency by Gulf Radiation Technology, July, 1970.

11. B. C. Passenheim, et al., "Study of Radiation Effects in Silicon Solar Cells", Final Report, Contract 952387 Prepared for the Jet Propulsion Laboratory, Pasadena, Calif., by Gulf Radiation Technology, January, 1971.

12. W. E. Horne, et al., "Real Time Space and Nuclear Effects (Accelerated Evaluation Techniques)", Final Report, Contract AFAPL-TR-72-69, Volume III (to be published).

13. Paul Hahn, "RSIC Computer Code Collection--Space Radiation Environment Shielding Systems (SPARES), CCC-148, AS-2807, Oak Ridge National Laboratory Radiation Shielding Information Center, Oak Ridge, Tenn., 1969.

14.   J. I. Vette, et al., NASA SP 3024, Vol. 1, 2, ..., 6 and NS SDC 72-06, 72-13, NASA Reports from 1965 to the present.

15.   J. Baicker, et al., Applied Physics Letters, 2, 104, 1963.

16.   T. Faith, "Temperature Dependence of Damage Coefficient in Electron Irradiated Solar Cells", IEEE Transactions on Nuclear Science, NS-14, 6, 82, 1967.

17.   J. R. Carter, "Effect of Electron Energy on Defect Introduction in Silicon", J. Phys. Chem. Solids, 27, 913, 1966.

18.   M. J. Barrett, "Electron Damage Coefficients in P-Type Silicon", IEEE Transaction on Nuclear Science, Vol. NS-14, No. 6, December, 1963.

19.   A. Meulenberg and F. C. Treble, "Damage in Silicon Solar Cells from 2 to 155 MeV Protons, " IEEE Photovoltaic Specialists Conference, Nov., 1973.
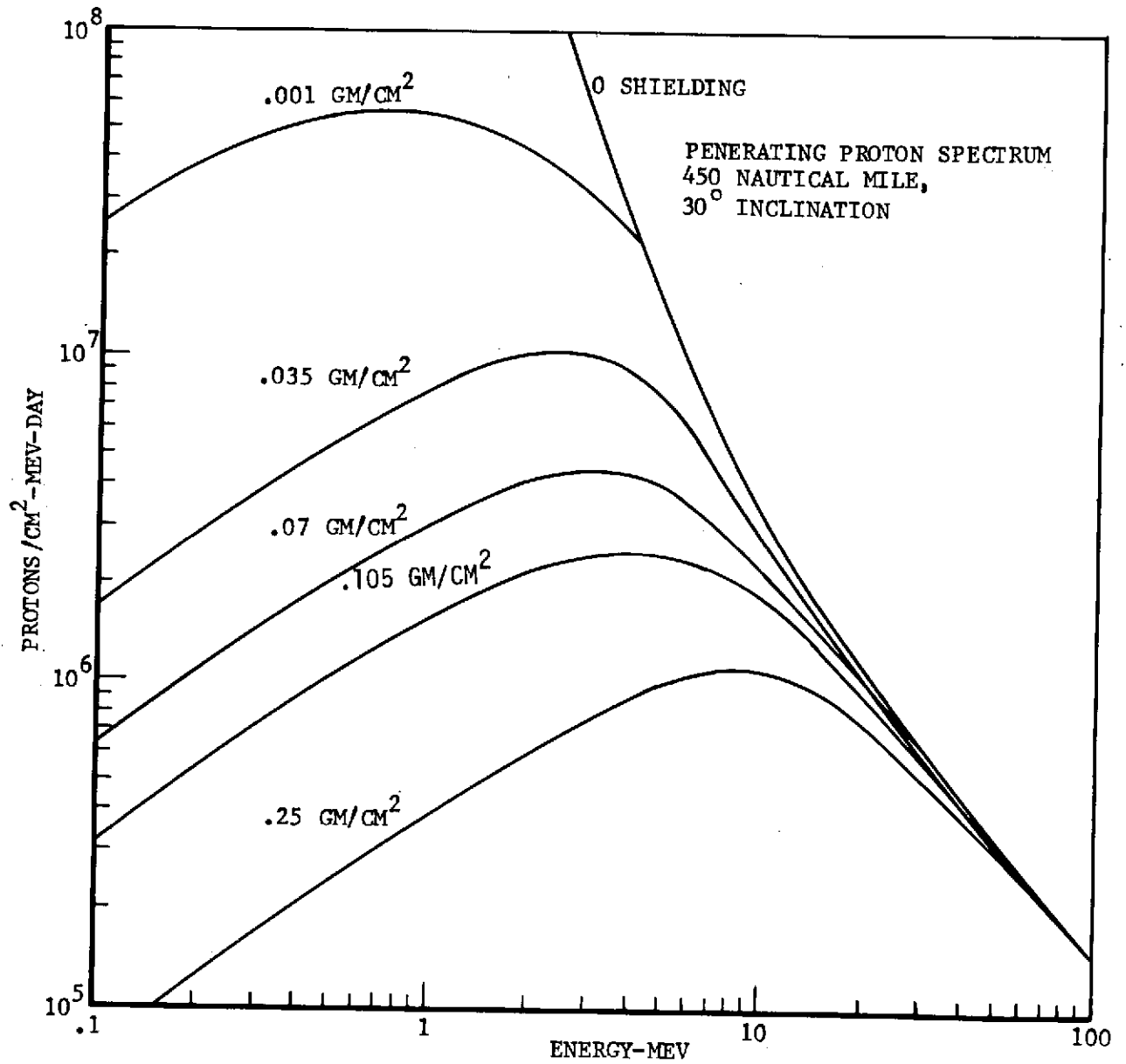
FIGURE 1: Typical Modified Spectrum Inside Solar Cell Structure
(450 NM 30° Inclination)
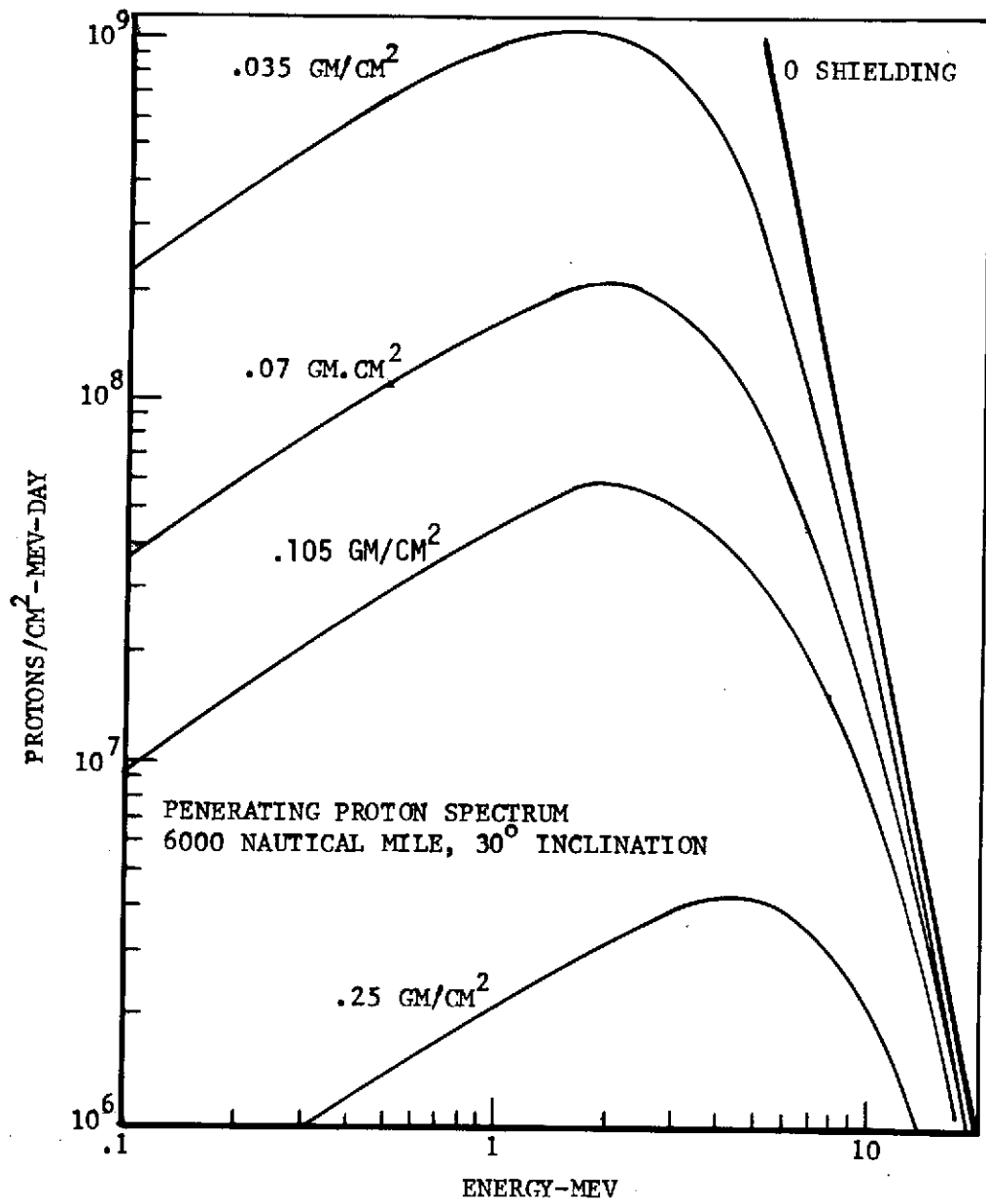
FIGURE 2: Typical Modified Spectrum Inside Solar Cell Structure
(6000 NM, 30° Inclination)
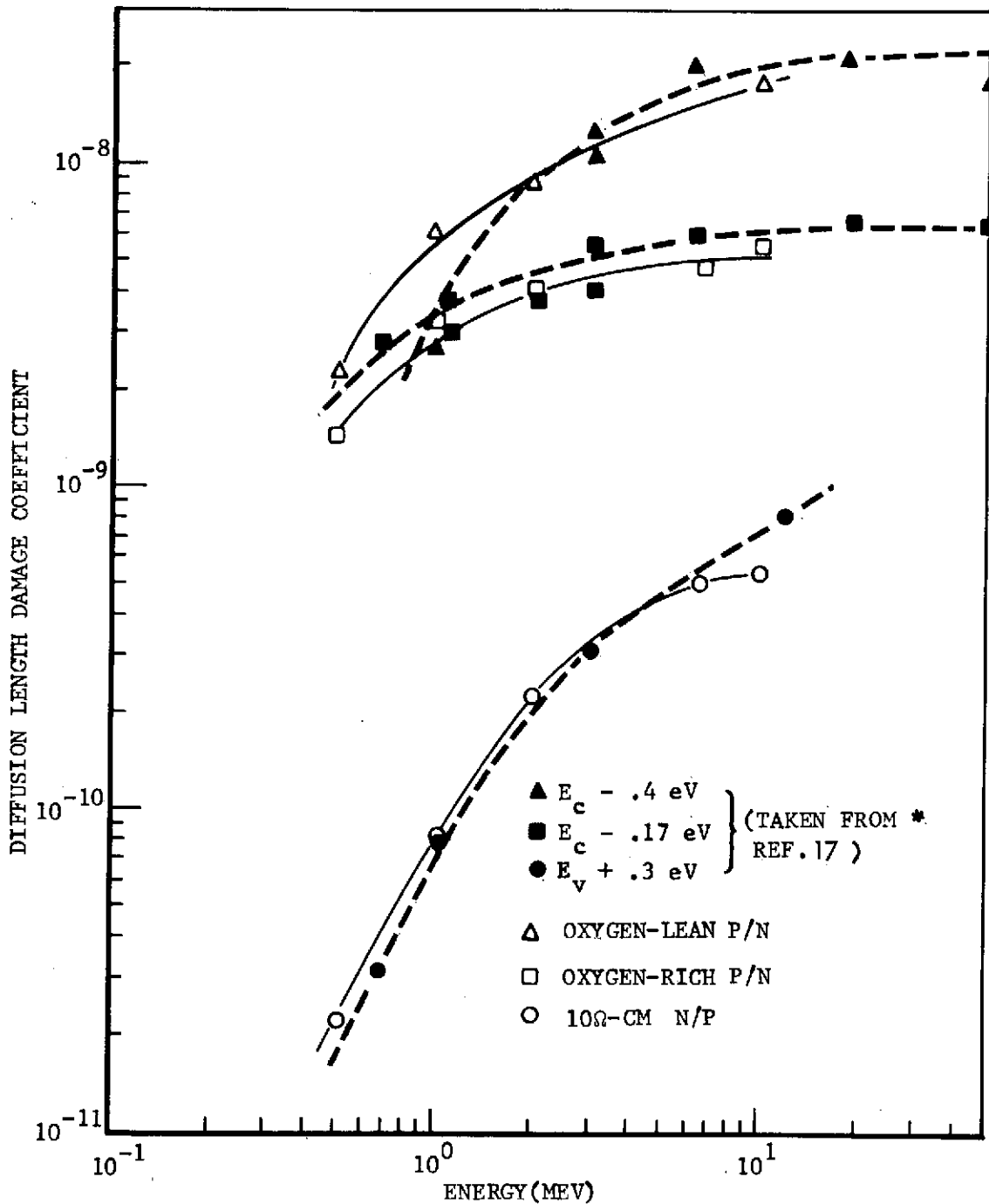
* (Note: Recombination Center Curves have been normalized
to respective damage coefficient curves.)

FIGURE 3: Comparison of Energy Dependence of Damage Coefficients
for Different Types of Solar Cells with the Energy
Dependence of Recombination Center Introduction Rates
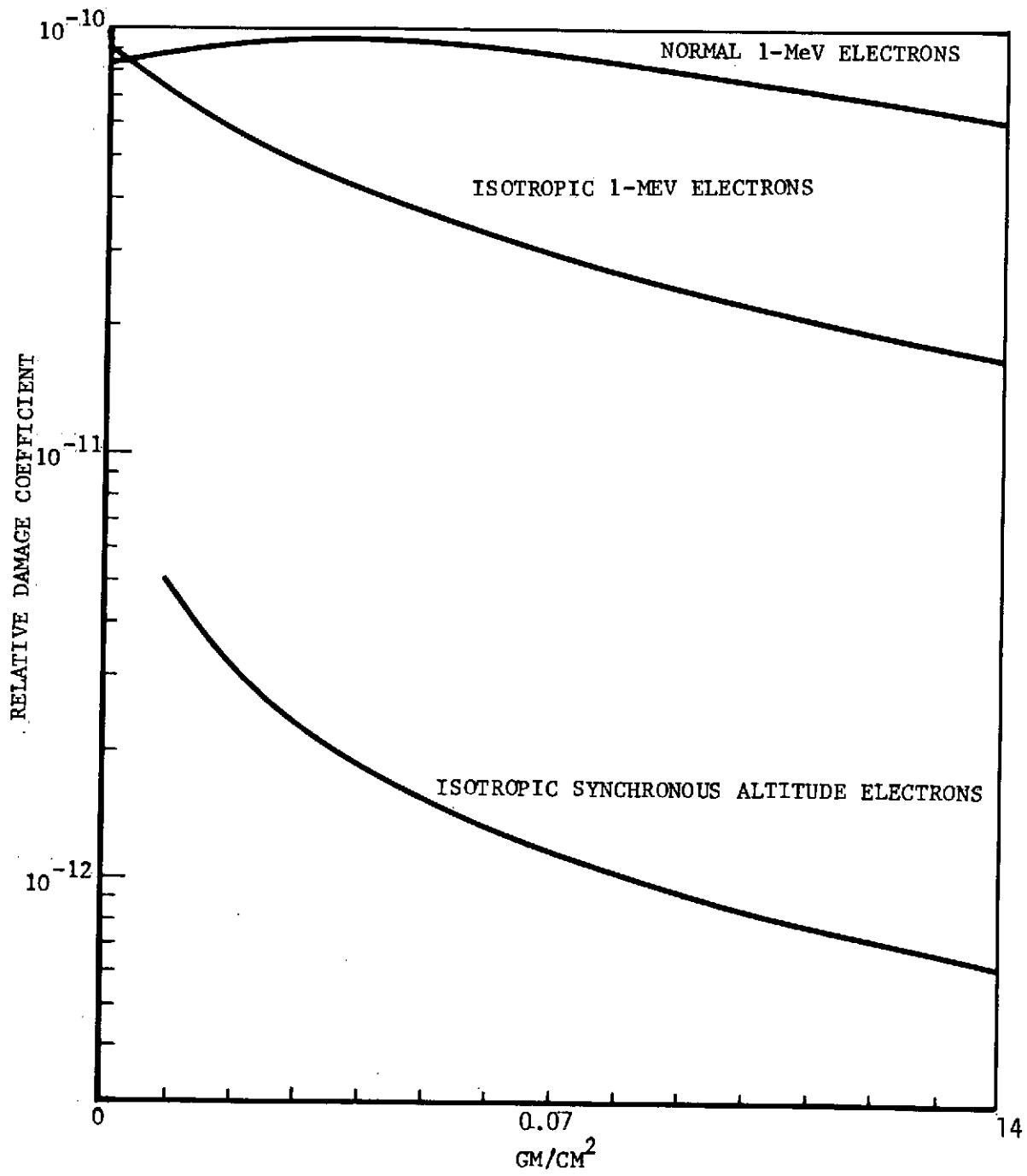
FIGURE 4: Typical Gradients of Defect Introduction Rate Through a Slab of Silicon
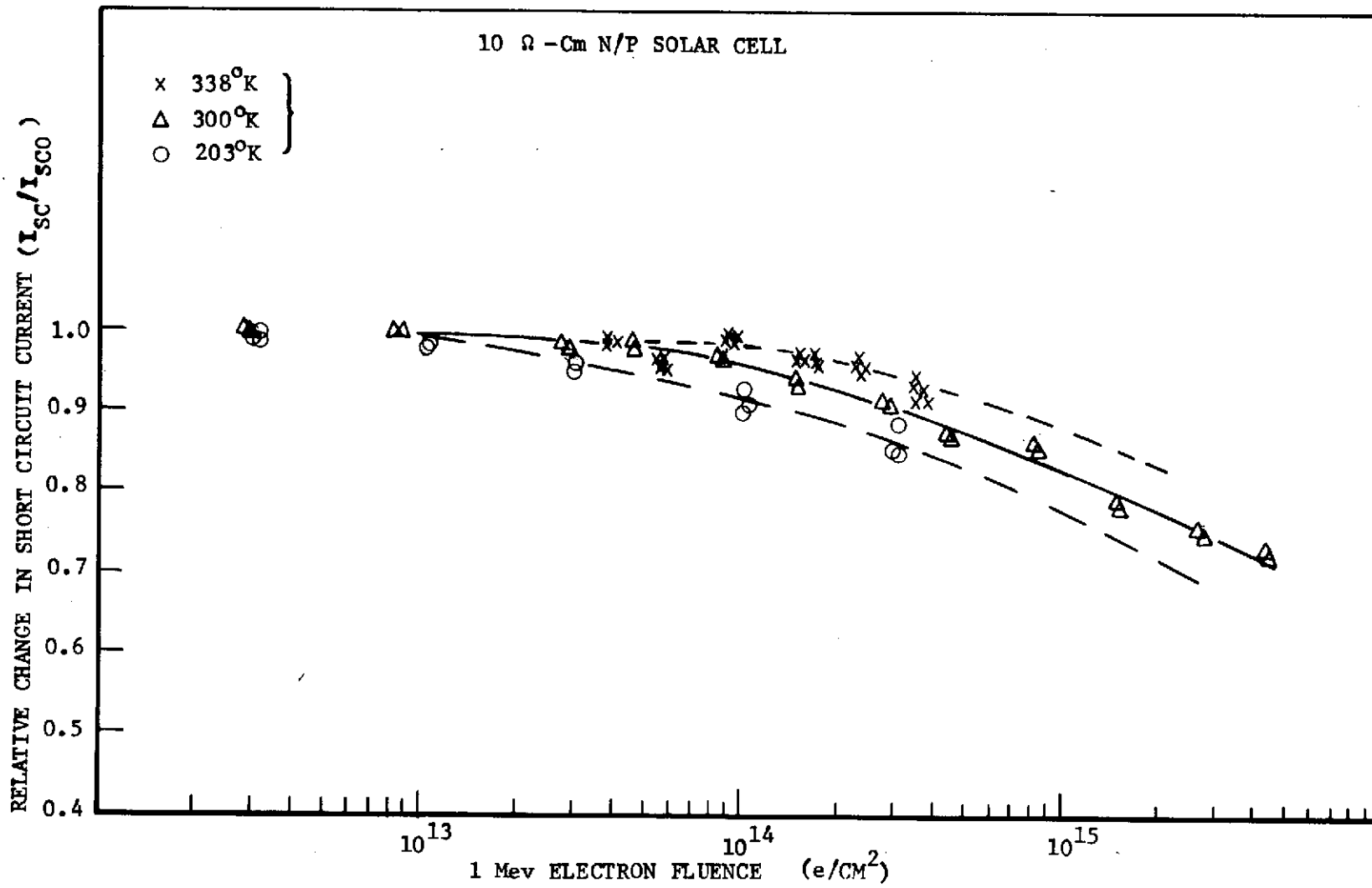
FIGURE 5 :   Temperature Dependence of 1-MeV Electron Degradation
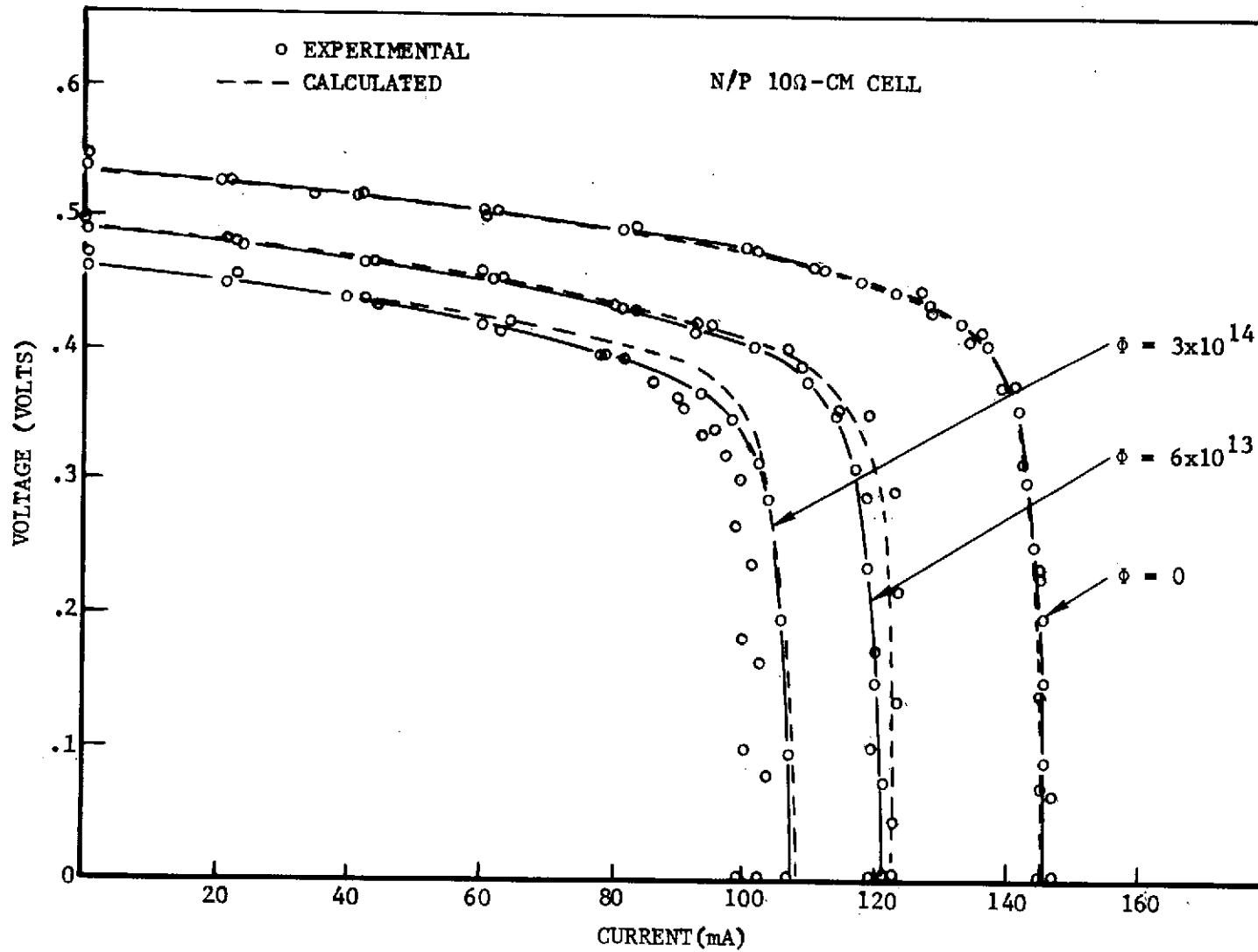
FIGURE 6 : Comparison of Calculated Versus Experimental 1-V Curves
for 10-MeV Electron
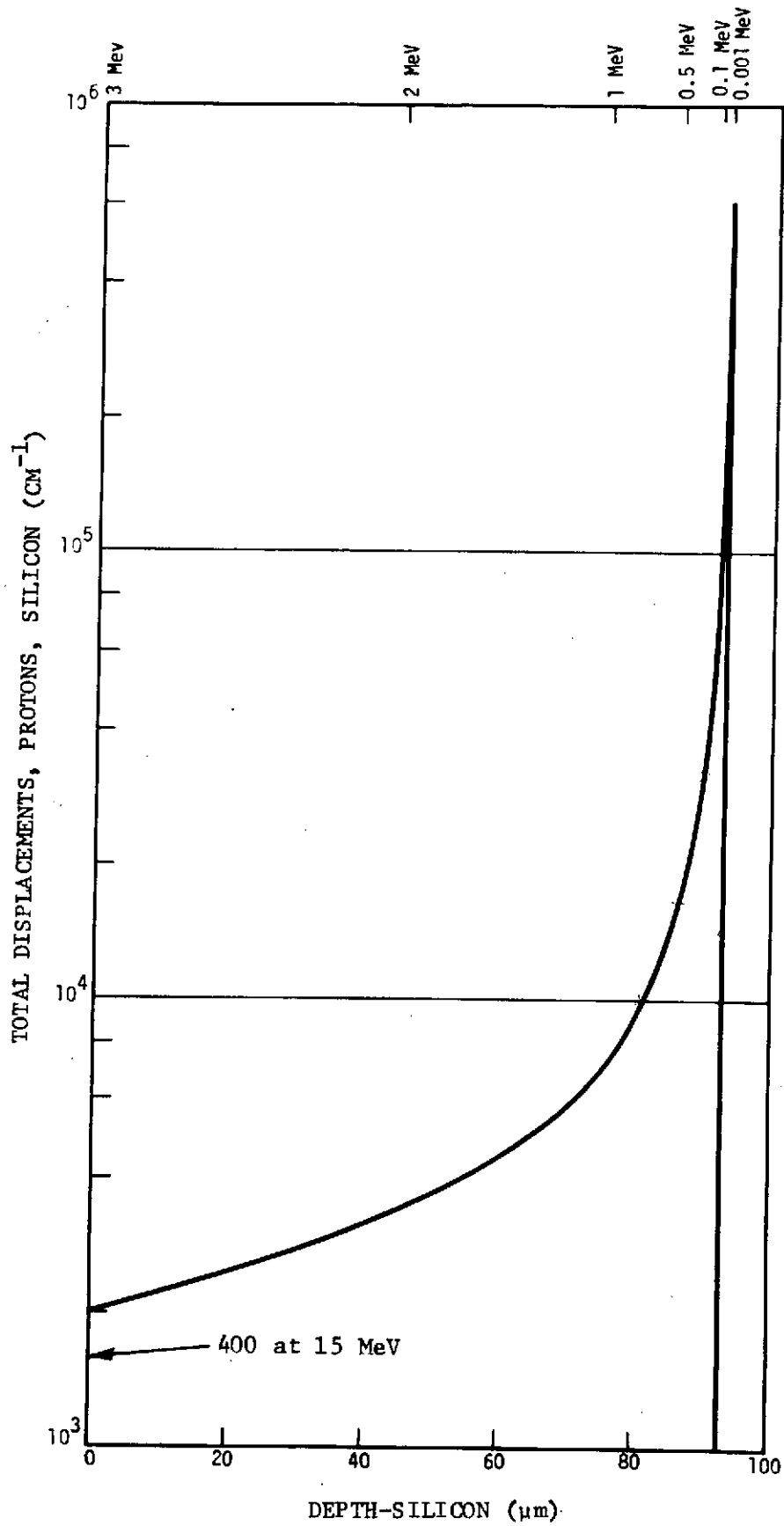
FIGURE 7: Atomic Displacements as a Function of Depth for a 3 MeV Proton in Silicon
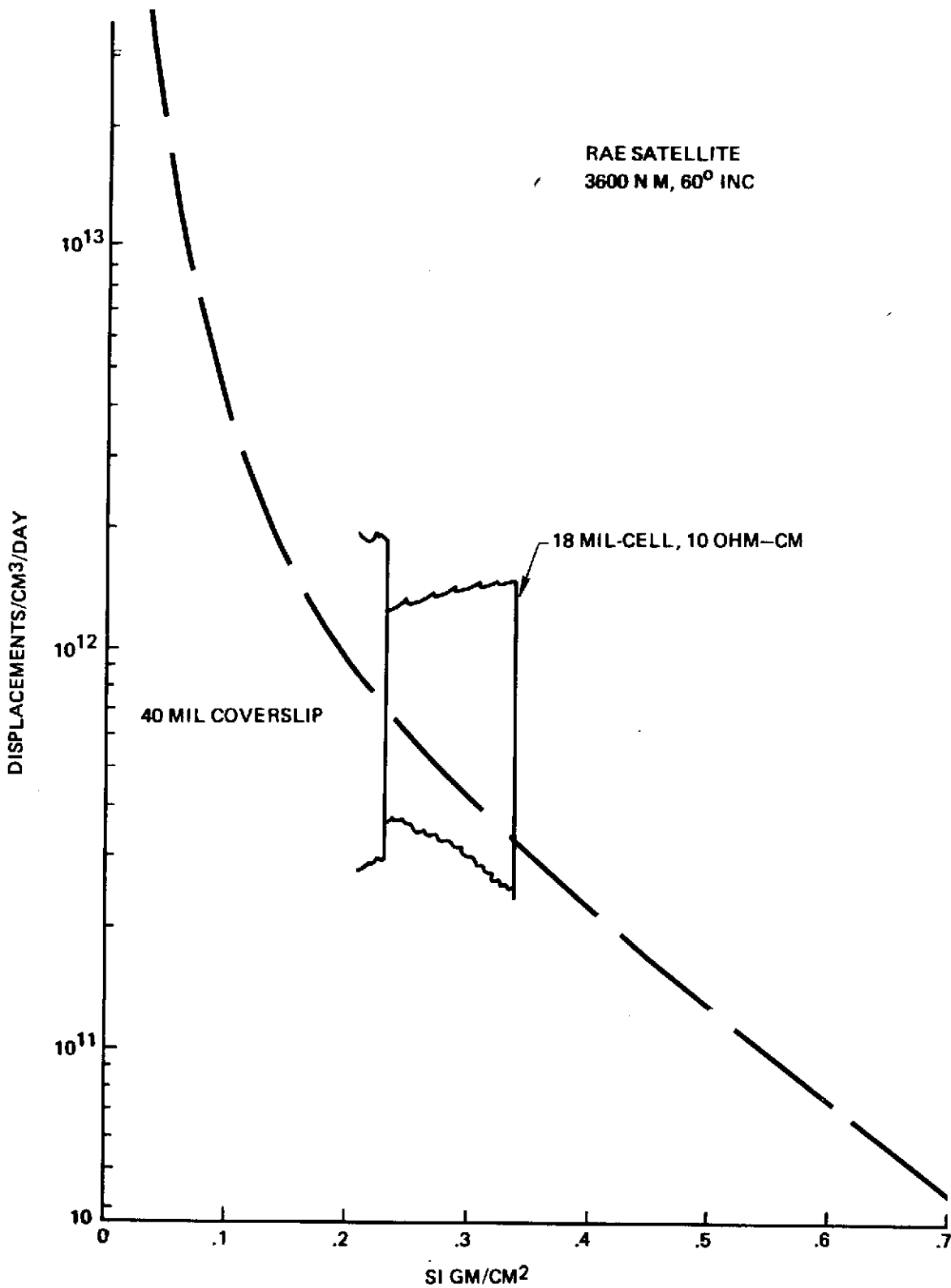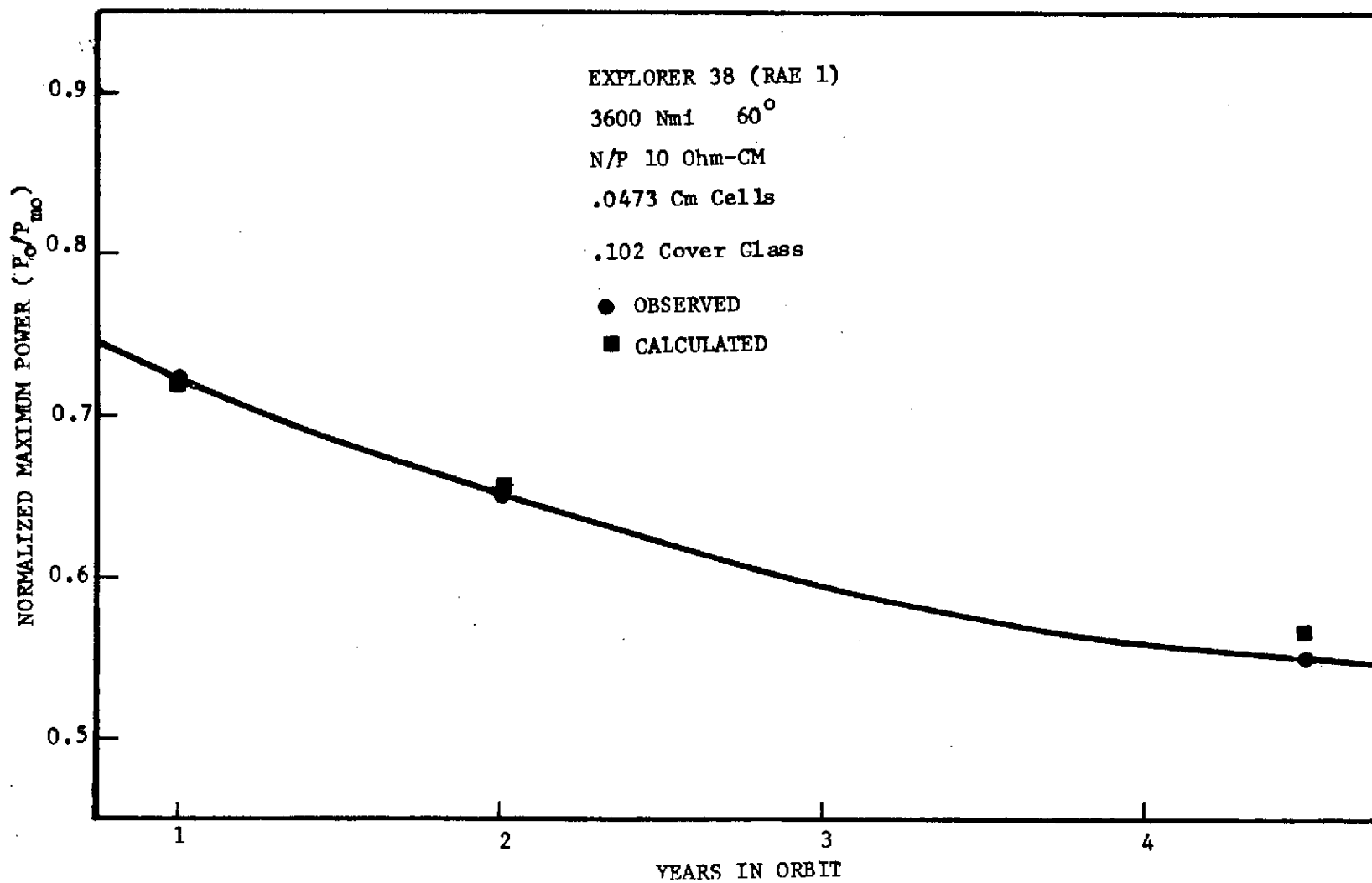
Figure 8: Displacement Damage Gradient for Explorer 38

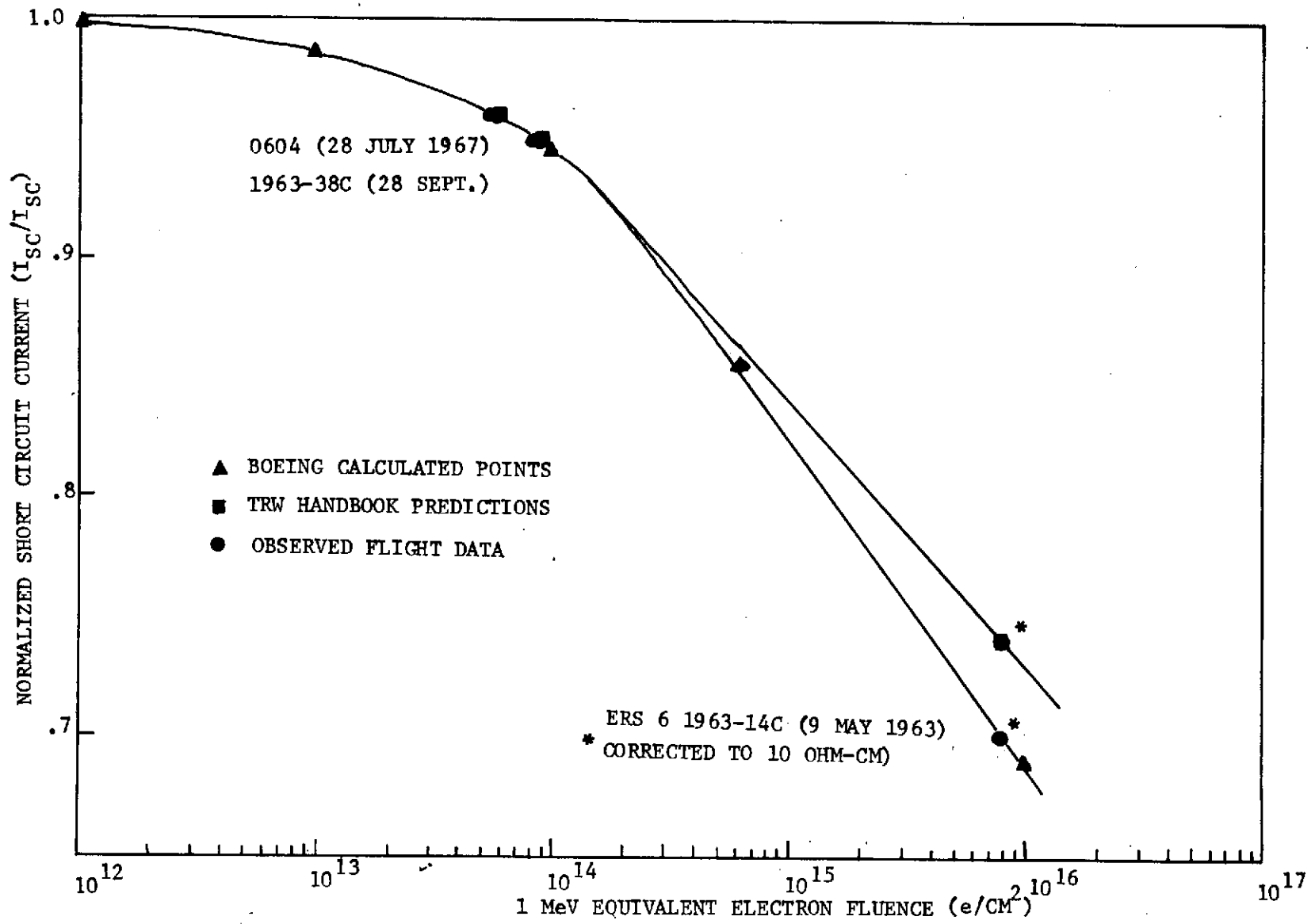FIGURE 9. Comparison of Calculated Versus Orbital Flight Results for RAE 1 Satellite

The figure shows a plot with the y-axis labeled "NORMALIZED MAXIMUM POWER (P_o/P_{mo})" ranging from 0.5 to 0.9, and the x-axis labeled "YEARS IN ORBIT" ranging from 1 to 4.

EXPLORER 38 (RAE 1)

3600 Nmi 60°

N/P 10 Ohm-CM

.0473 Cm Cells

.102 Cover Glass

● OBSERVED

■ CALCULATED

31

FIGURE 10 . 0604, 1963-38C, & ERS Flight Data & Predictions

- Y-axis: NORMALIZED SHORT CIRCUIT CURRENT (I_{SC}/I_{SC})
- X-axis: 1 MeV EQUIVALENT ELECTRON FLUENCE (e/CM^2)

Legend:
- ▲ BOEING CALCULATED POINTS
- ■ TRW HANDBOOK PREDICTIONS
- ● OBSERVED FLIGHT DATA

Annotations on plot:
0604 (28 JULY 1967)
1963-38C (28 SEPT.)

ERS 6 1963-14C (9 MAY 1963)
* CORRECTED TO 10 OHM-CM)
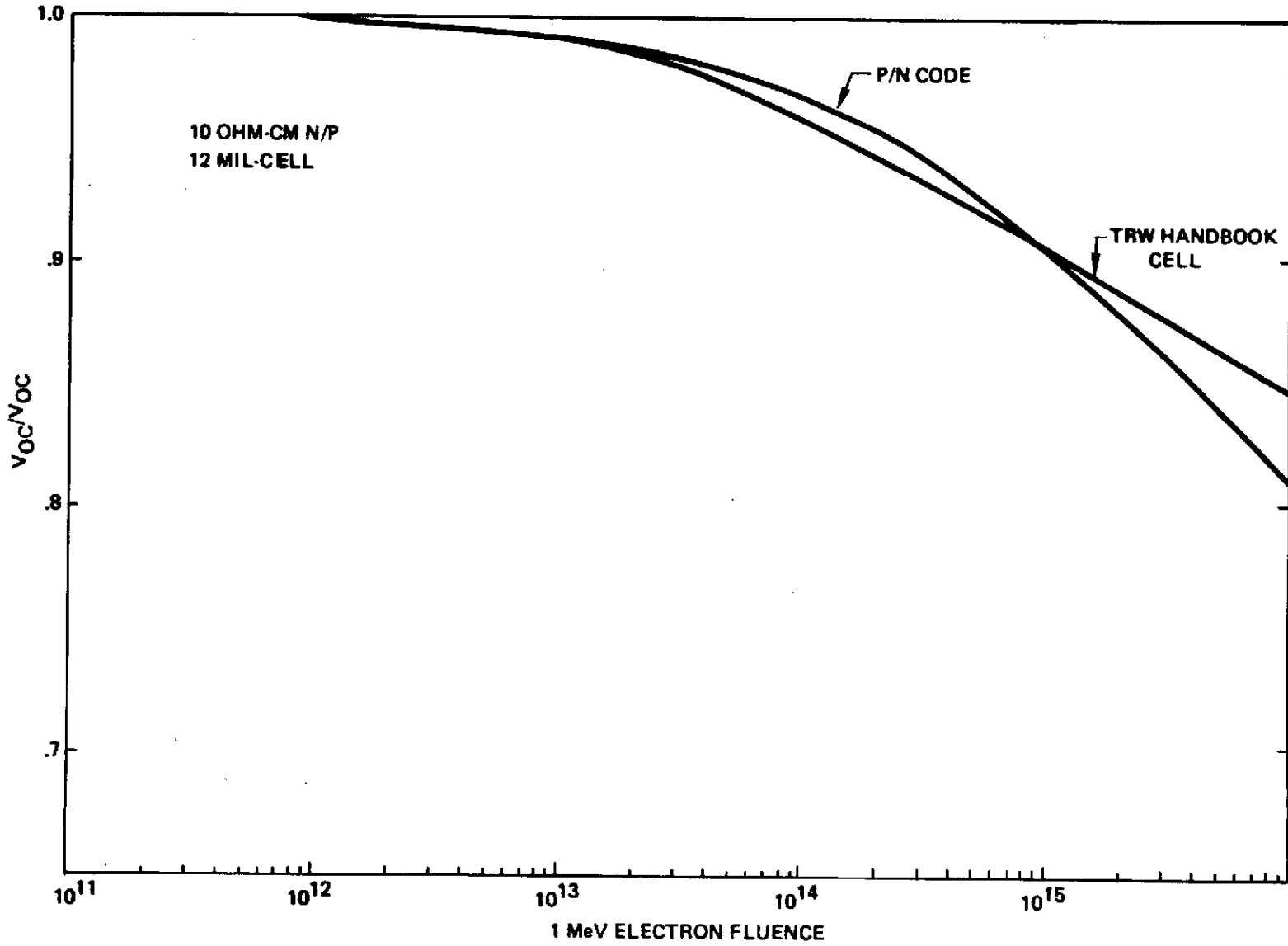
Figure 11: Boeing P-N & TRW Nominal Cell V_{OC} Degradation
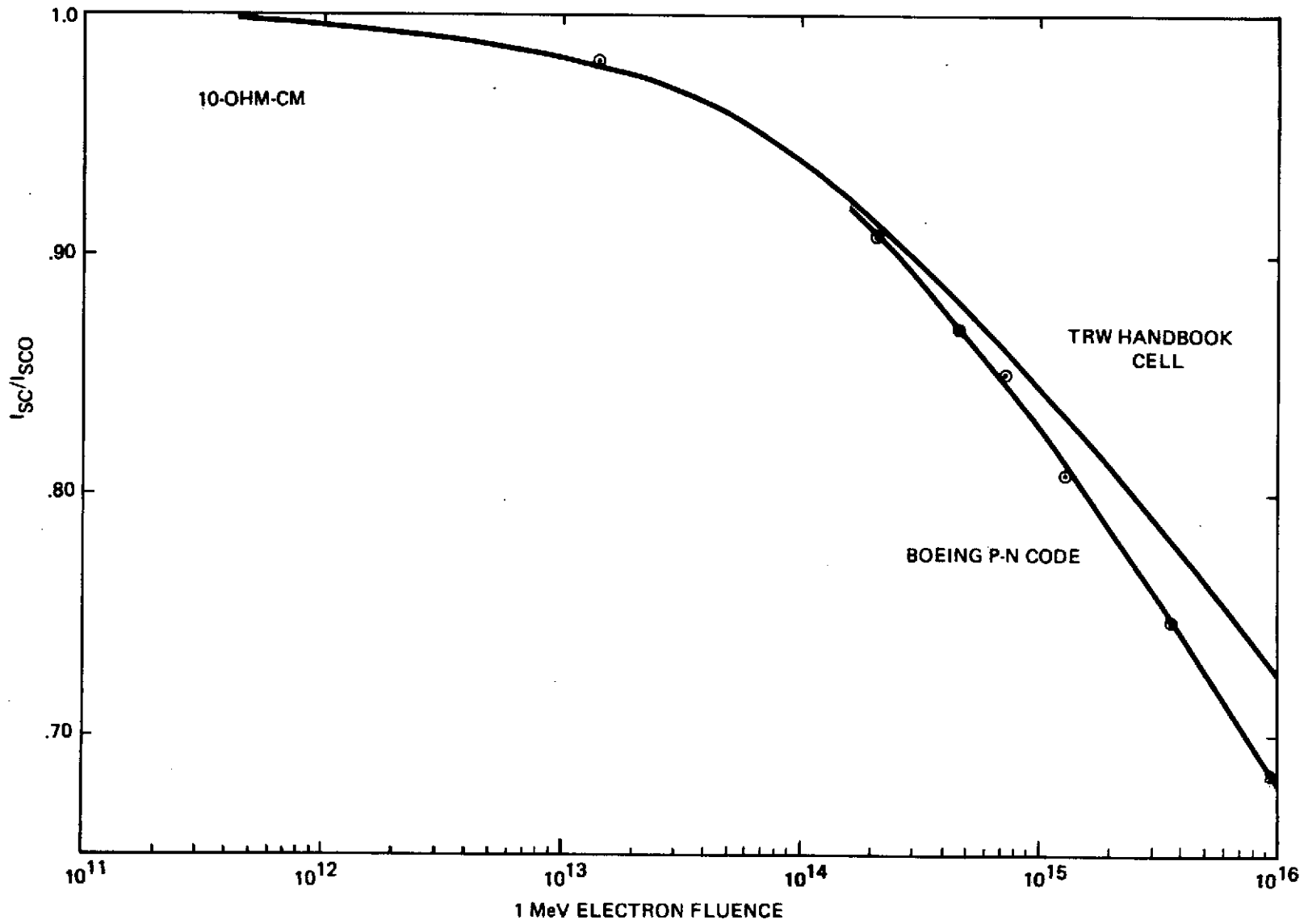
Figure 12: *Boeing P-N & TRW Nominal I_{SC} Degradation*
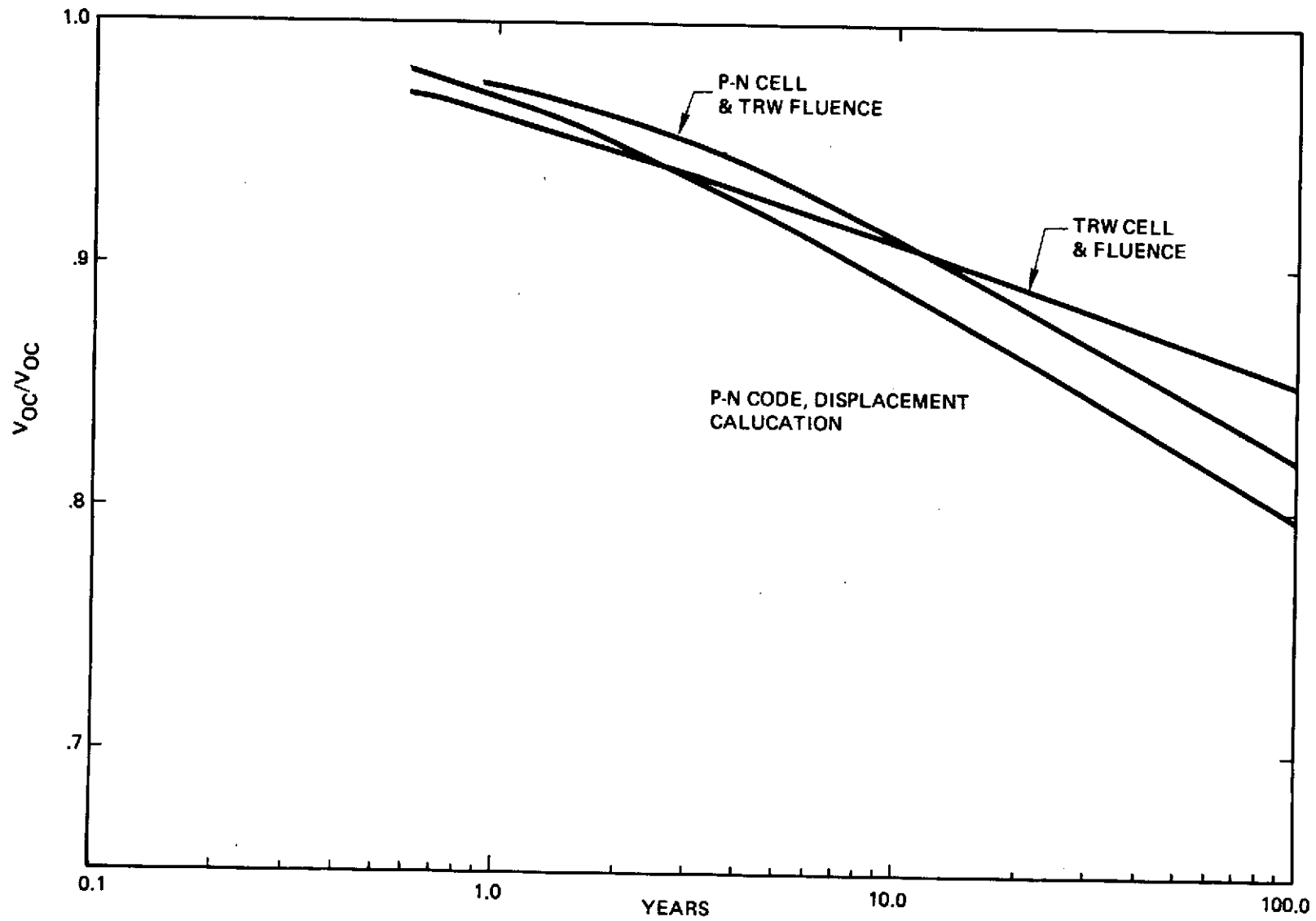
Figure 13: 450 NM V_OC Degradation Comparison
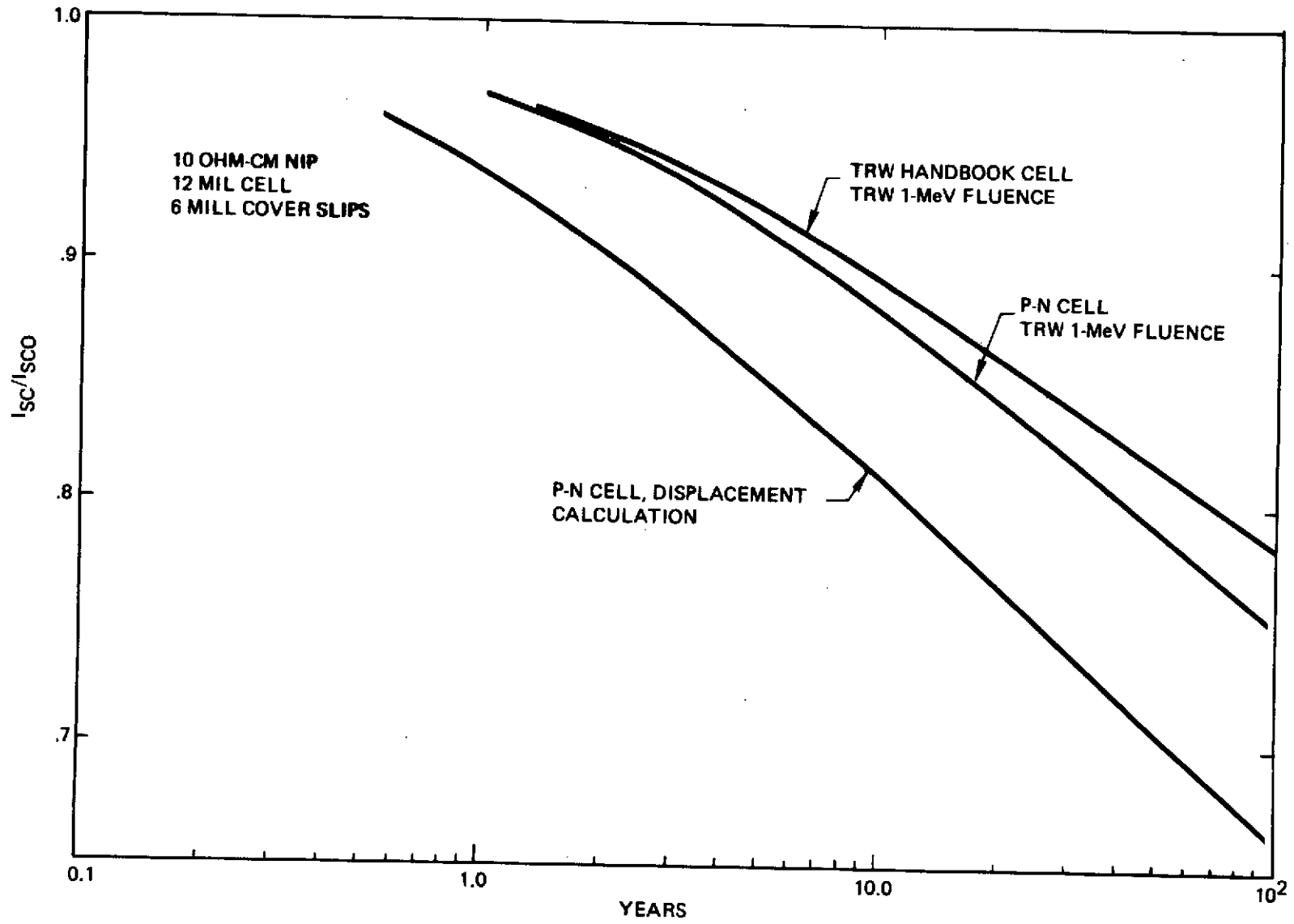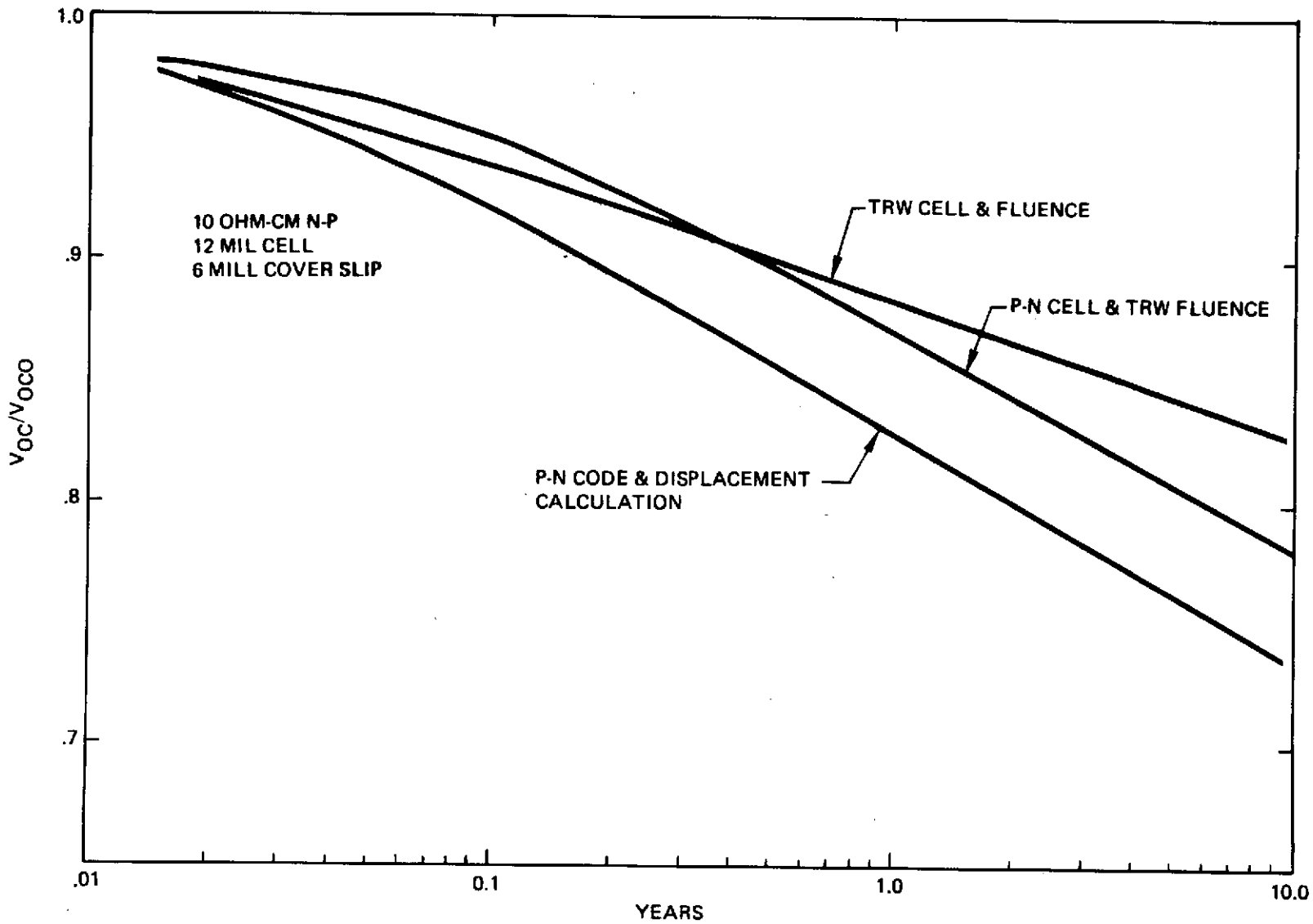
Figure 14: *450 NM I_{SC} Degradation Comparison*

The figure shows a plot with I_{SC}/I_{SCO} (labeled as %) on the vertical axis ranging from .7 to 1.0, and YEARS on the horizontal axis ranging from 0.1 to 10^2.

Annotations on the plot:
- 10 OHM-CM NIP
- 12 MIL CELL
- 6 MILL COVER SLIPS
- TRW HANDBOOK CELL / TRW 1-MeV FLUENCE
- P-N CELL / TRW 1-MeV FLUENCE
- P-N CELL, DISPLACEMENT CALCULATION

Figure 15: 6000 NM V_{OC} Degradation Comparison
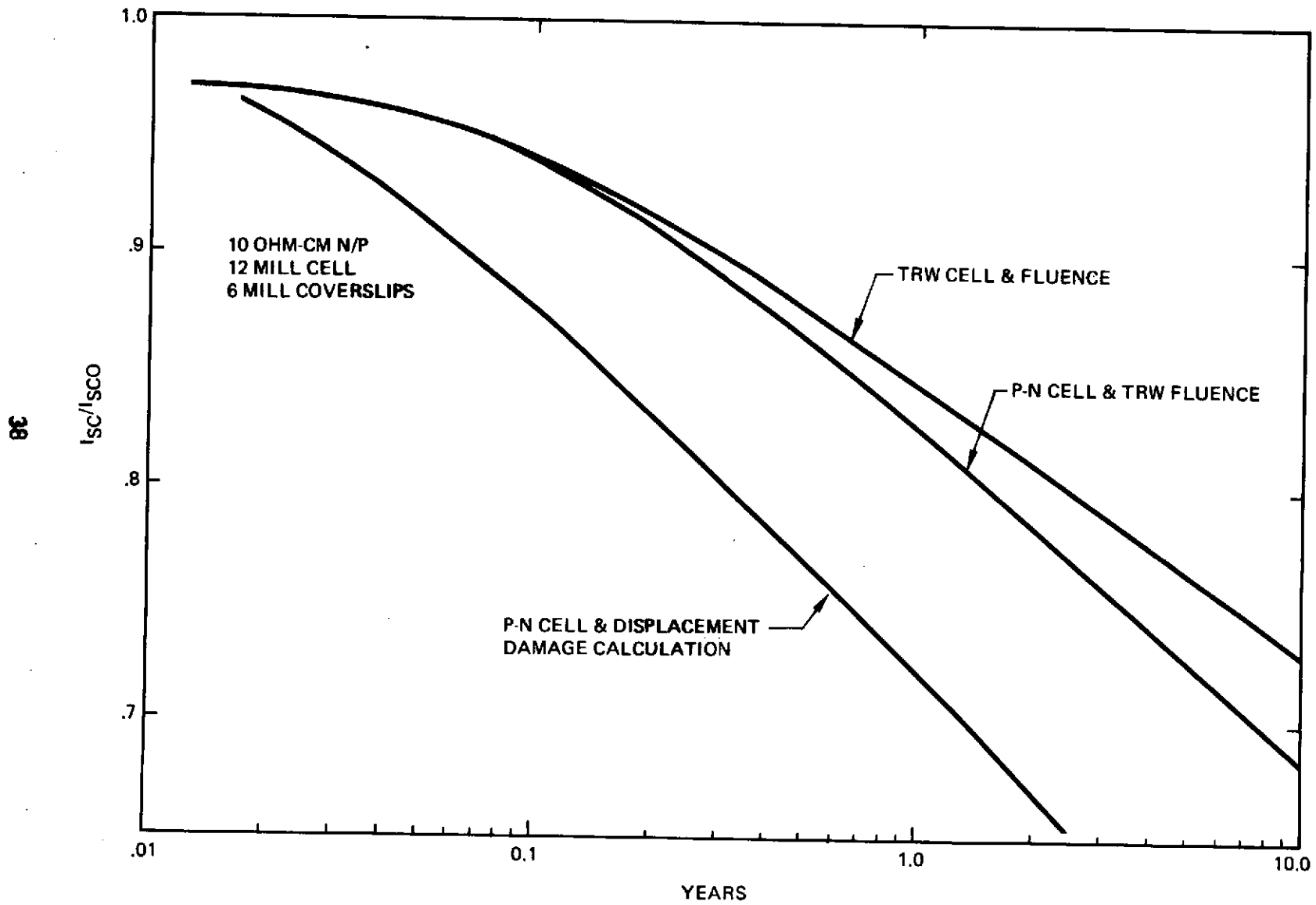
Figure 16: 6000 NM I_{SC} Degradation Comparison

The chart contains the following labels:

- I_{SC}/I_{SCO} (y-axis)
- YEARS (x-axis)
- 10 OHM-CM N/P
- 12 MILL CELL
- 6 MILL COVERSLIPS
- TRW CELL & FLUENCE
- P-N CELL & TRW FLUENCE
- P-N CELL & DISPLACEMENT DAMAGE CALCULATION

Axis values: 1.0, .9, .8, .7 (y-axis); .01, 0.1, 1.0, 10.0 (x-axis)
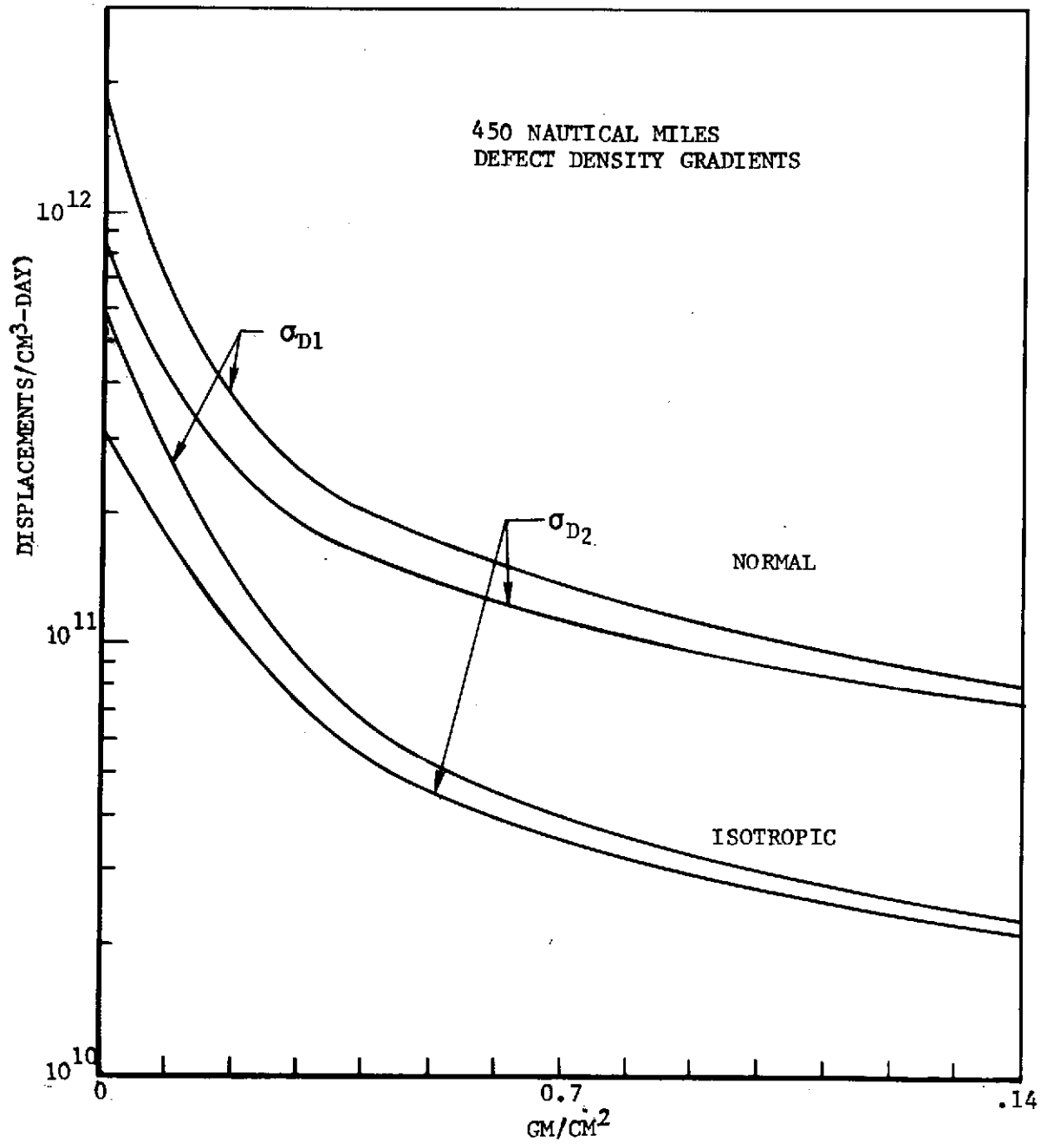
FIGURE 17 : Typical Displacement Density Gradient Inside Solar Cell Due
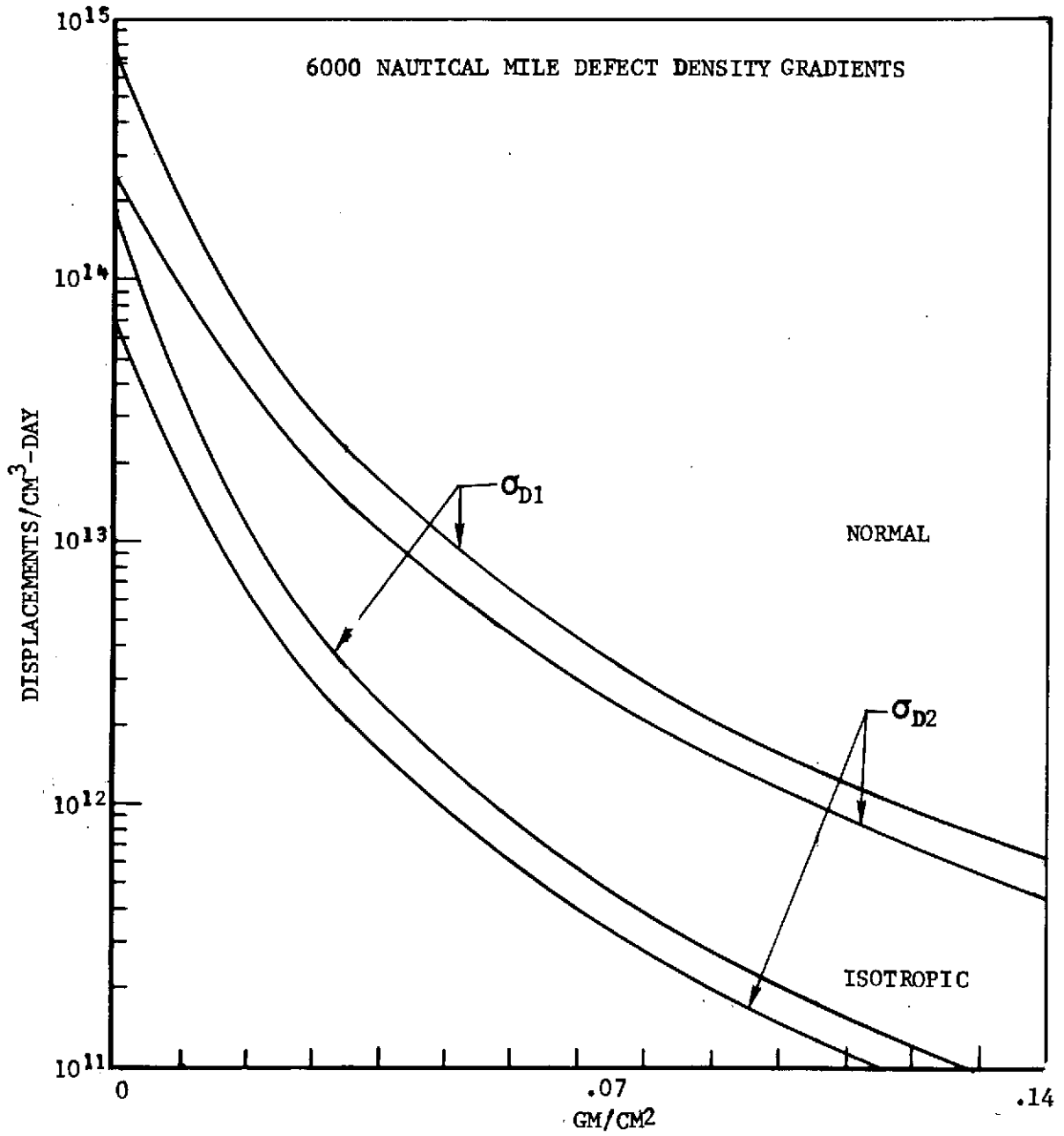to Space Spectrum (450 NM)

39

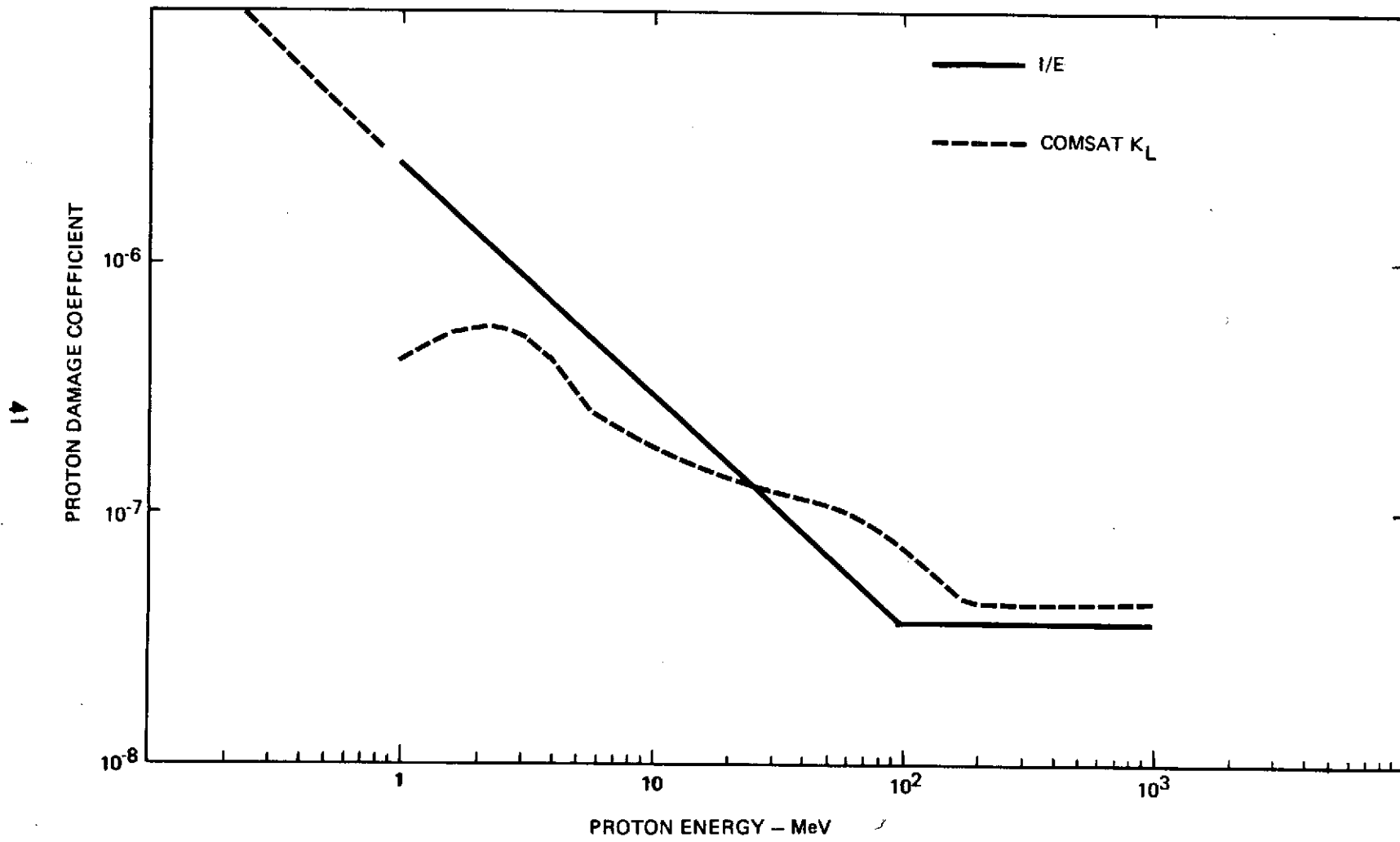FIGURE 18. Typical Displacement Density Gradient Inside Solar Cell Due to Space Spectrum (6000 NM)

Figure 19: Damage Coefficient Comparison